Ocean Sci., 21, 1909–1931, 2025
https://doi.org/10.5194/os-21-1909-2025

Ocean Science Open Access EGU

Far-future climate projection of the Adriatic marine heatwaves: a kilometre-scale experiment under extreme warming

Cléa Denamiel[1,2]

[1]Ruđer Bošković Institute, Division for Marine and Environmental Research, Bijenička cesta 54, 10000 Zagreb, Croatia
[2]Institute for Adriatic Crops and Karst Reclamation, Put Duilova 11, 21000 Split, Croatia

Correspondence: Cléa Denamiel (cdenami@irb.hr)

Received: 22 March 2025 – Discussion started: 3 April 2025
Revised: 19 June 2025 – Accepted: 30 June 2025 – Published: 4 September 2025

Abstract. The impact of a far-future extreme warming scenario on Adriatic marine heatwave (MHW) characteristics – including intensity, duration, spatial extent, and associated environmental drivers – is assessed using the Adriatic Sea and Coast (AdriSC) kilometre-scale atmosphere–ocean model. The main aim of this study is to evaluate the added value and limitations of the pseudo-global-warming (PGW) approach, used to force the far-future AdriSC simulation, in projecting Adriatic MHWs. In line with existing knowledge, the results indicate a significant increase in MHW intensity along with a notable expansion in spatial coverage, particularly in the central and eastern Adriatic. Seasonal patterns show that the most intense MHWs occur between May and September, with events extending into late autumn and early winter under extreme warming. This study also reveals several novel insights. First, the Po River plume is identified as a key factor for the onset and decline of MHWs. Lower river discharges are associated with intense MHW onset, while higher discharges aid in heat dissipation during decline phases. As air–sea heat fluxes are demonstrated to play a critical role in MHW onset along the plume, these findings suggest that MHWs are more likely to develop and persist under low Po River discharge conditions, when water clarity increases and solar radiation absorption is enhanced due to reduced suspended sediments and organic matter. Second, the study identifies a gap in MHW activity, potentially linked to the Eastern Mediterranean Transient, highlighting the influence of natural variability on MHW dynamics. However, no correlation is found with the Ionian–Adriatic Bimodal Oscillating System, suggesting the need for further research on oceanographic influences. Consequently, the PGW approach is found to effectively capture the thermodynamic changes influencing the MHWs in the Adriatic Sea despite potentially oversimplifying future MHW dynamics as it assumes stationarity in climate signals. Finally, these findings underscore the urgent need for adaptive strategies to mitigate the impacts of intensified MHWs on marine ecosystems and coastal communities, particularly in vulnerable nearshore areas. Future research should incorporate ensembles of high-resolution projections and assess additional climate stressors to provide a more comprehensive understanding of Adriatic MHWs under future warming.

1 Introduction

In the Mediterranean basin, the past decade has witnessed an alarming escalation in extreme heatwave events, both on land and in the sea (Pastor et al., 2024). These heatwaves have soared beyond historical norms, with their unprecedented scale posing significant challenges to ecosystems and human societies alike. In particular, Tejedor et al. (2024) have highlighted the alarming potential of anthropogenic climate change to transform rare, extreme atmospheric heatwaves – once characterized by 10 000-year return periods, such as those observed in 2023 and 2024 in the Mediterranean – into regular occurrences happening as frequently as every 4 years under extreme warming scenarios. This startling shift not only threatens to exceed the adaptive capacity of human populations in the Mediterranean basin, as emphasized by Masselot et al. (2025) and Bujosa Mateu et al. (2024), but also carries profound consequences for oceanic ecosystems. Such marine impacts include habitat degradation, biodiver-

sity loss, and shifts in ecological dynamics, as previously noted by Smale et al. (2019).

Recent studies underscore the importance of utilizing high-resolution datasets capable of resolving mesoscale and sub-mesoscale processes, such as downwelling caused by eddies or waves, to comprehensively evaluate the impacts of marine heatwaves (MHWs) from the surface to the subsurface layers (Dayan et al., 2022; Garrabou et al., 2022). These datasets are essential not only for identifying the role of MHWs in triggering mortality events (Garrabou et al., 2019; Smith et al., 2024) but also for addressing the specific needs of local stakeholders, such as aquaculture farms, which are highly sensitive to localized oceanic temperature changes (Zemunik Selak et al., 2024). Despite this, a standardized best practice for selecting models or reanalyses capable of accurately depicting MHW events at sub-regional and local scales remains elusive.

In this context, the relevance of the pseudo-global-warming (PGW) approach (Schär et al., 1996; Denamiel et al., 2020a) becomes particularly evident. This method involves modifying existing reanalysis datasets by superimposing climatological differences between historical and future regional or global climate simulations to drive high-resolution coastal models at kilometre-scale resolutions. In the atmosphere, this approach has already proven effective in capturing the substantial increase in heatwave frequency, duration, and intensity projected under future scenarios. Applications of the PGW methodology in this context have provided valuable insights across Europe (e.g. Fischer and Schär, 2010), Asia (e.g. Imada et al., 2019), and North America (e.g. Patricola and Wehner, 2018), where it accounts for localized feedback mechanisms such as soil moisture depletion and urban heat island effects. However, a key limitation of the PGW approach lies in its assumption of stationarity in the climate signal, which risks oversimplifying evolving climate dynamics. This limitation is particularly significant for phenomena governed by nonlinear climate change processes, as highlighted by Brogli et al. (2023).

The PGW approach has predominantly been applied to atmospheric studies and this gap in research underscores the necessity of evaluating its effectiveness in modelling MHWs. Understanding whether this approach can accurately simulate the oceanic conditions associated with MHWs is crucial, as it would enable researchers to assess the impacts of climate change on marine ecosystems and coastal communities more effectively. Given the increasing frequency and severity of Mediterranean MHWs, as highlighted by recent studies (Martín et al., 2024), applying the PGW methodology to marine environments could provide valuable insights into future oceanic conditions under various climate scenarios. This advancement would enhance the research community capacity to predict and mitigate the adverse effects of MHWs on marine biodiversity and human activities dependent on marine resources.

In this study, the kilometre-scale Adriatic Sea and Coast (AdriSC) climate model (Denamiel et al., 2019; Fig. 1) is thus used to understand how the PGW approach compares to traditional downscaling methods in terms of the characterization of the marine heatwaves within the Adriatic basin. The ability of the AdriSC model to simulate the present and future decadal atmosphere–ocean dynamics has already been assessed, with many studies demonstrating the added value of such a kilometre-scale approach (Denamiel et al., 2020a, b, 2021a, b, 2022, 2025; Pranić et al., 2021, 2023, 2024; Tojčić et al., 2023, 2024). Consequently, the present study focuses on analysing and characterizing in detail the far-future impacts of an extreme warming scenario on the Adriatic MHW events. The article is structured as follows. Section 2 describes the AdriSC model and the analytical methods used, Sect. 3 assesses and discusses the impacts of climate change on Adriatic MHW events from the basin to the subdomain scales, Sect. 4 evaluates the strengths and limitations of the PGW approach for characterizing far-future MHW, and Sect. 5 presents the main conclusions of the study.

2 Model and methods

2.1 Adriatic Sea and Coast (AdriSC) model

The Adriatic Sea and Coast (AdriSC) climate model (Denamiel et al., 2019) was designed to enhance the representation of atmospheric and oceanic dynamics within the Adriatic basin, offering improved modelling of the local processes compared to existing Mediterranean regional climate system models (RCSMs). Built on the Coupled Ocean–Atmosphere–Wave–Sediment Transport (COAWST) framework (Warner et al., 2010), it couples the Weather Research and Forecasting (WRF; Skamarock et al., 2005) atmospheric model with the Regional Ocean Modeling System (ROMS; Shchepetkin and McWilliams, 2009). In the AdriSC climate simulations, as described and illustrated in Denamiel et al. (2025) and Fig. 1, the WRF model employs two nested grids with 15 and 3 km resolutions, while ROMS utilizes grids with 3 and 1 km resolutions. The model uses vertical terrain-following coordinates, with 58 atmospheric levels refined near the surface (Laprise, 1992) and 35 oceanic levels optimized near the sea surface and ocean floor (Shchepetkin and McWilliams, 2009).

The AdriSC suite is implemented and rigorously validated on the high-performance computing infrastructure of the European Centre for Medium-Range Weather Forecasts (ECMWF). Additional details about its configuration are available in Denamiel et al. (2019, 2021a) and Pranić et al. (2021).

This research evaluates the effects of climate change on MHWs using two 31-year AdriSC climate simulations: a historical simulation spanning 1987–2017 and a far-future extreme warming scenario for 2070–2100 based on Represen-

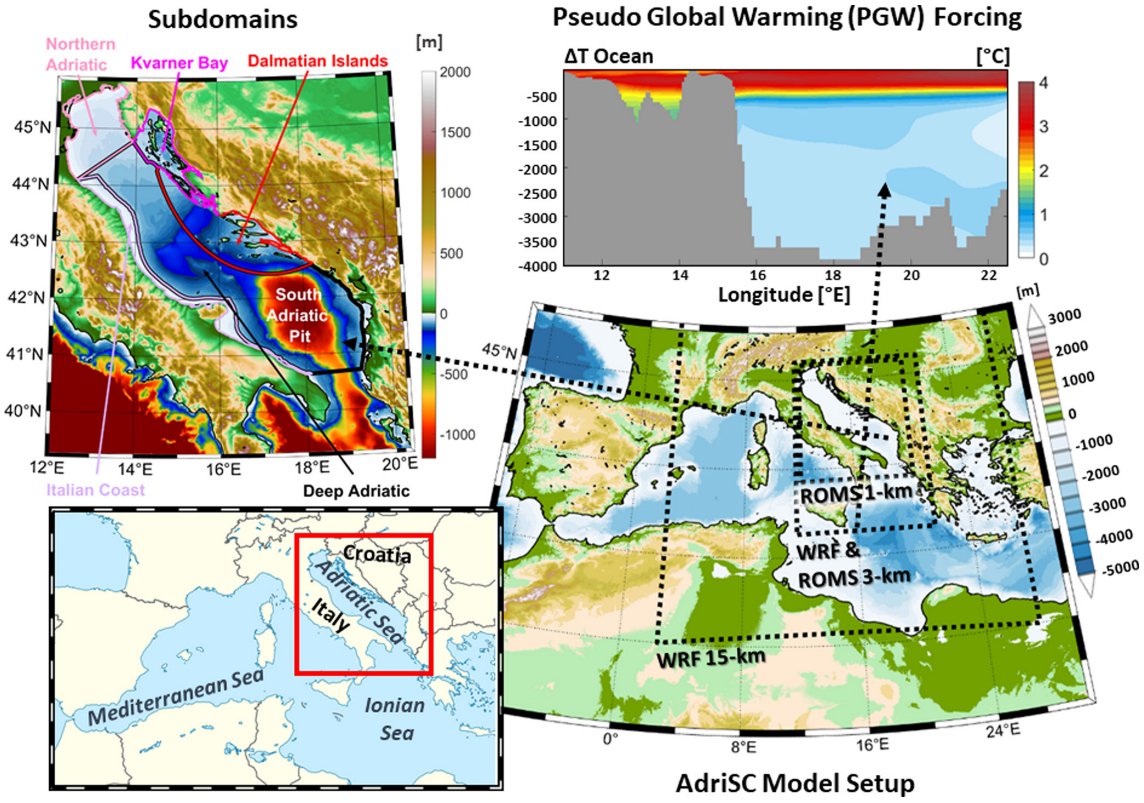

Figure 1. Spatial coverage and horizontal resolution of the different grids used in the AdriSC climate model setup including the topo-bathymetry of the AdriSC 1 km model with the locations of the five subdomains (coloured polygons) used in this study and the pseudo-global-warming temperature ocean forcing imposed in the AdriSC 3 km model southern boundary for the extreme warming simulation.

tative Concentration Pathway (RCP) 8.5 (referred to as the RCP8.5 simulation).

For the historical run, initial and boundary conditions are provided to the WRF 15 km model using 6-hourly ERA-Interim reanalysis data at 0.75° resolution (Dee et al., 2011) and to the ROMS 3 km model using MEDSEA reanalysis from the Mediterranean Forecasting System at 1/16° resolution (Simoncelli et al., 2019). Prior evaluations of the AdriSC historical run confirm its ability to accurately replicate the Adriatic's multi-decadal dynamics (Denamiel et al., 2022, 2025; Pranić et al., 2021, 2024).

2.2 PGW methodology

As described and illustrated in Denamiel et al. (2025) and Fig. 1, for the RCP8.5 simulation, the PGW approach (Schär et al., 1996; Denamiel et al., 2020a) is used to adjust the historical forcing dataset by incorporating climatological changes from the LMDZ4-NEMOMED8 RCSM (Hourdin et al., 2006; Beuvier et al., 2010). Specifically, atmospheric variables such as air temperature, relative humidity, and wind components from ERA-Interim are modified using differences between the 2070–2100 and 1987–2017 periods under RCP8.5 (ΔT, ΔRH, ΔU, and ΔV, respectively). These changes generate 6-hourly three-dimensional atmospheric forcing for all 366 d of the year, which are then applied to the WRF 15 km model in the PGW simulation. Similarly, oceanic variables, including temperature, salinity, and currents, are adjusted using the climatological differences to produce daily three-dimensional oceanic forcing for ROMS 3 km (ΔT ocean, ΔS ocean, ΔU ocean, and ΔV ocean, respectively). This process ensures that each simulated year inherits the synoptic conditions of the historical reanalysis while embedding the projected climatological shifts.

However, the PGW approach has several limitations, including simplified atmosphere–ocean dynamics, the assumption of stationarity, perturbations in initial and boundary conditions, resolution constraints, and neglected feedback mechanisms.

The PGW method used in the AdriSC climate model to predict MHWs in the Adriatic Sea incorporates both thermodynamic changes – such as temperature, salinity, and humidity – and dynamic adjustments (i.e. wind and ocean currents). Consequently, the inaccuracies in representing circulation patterns critical for heatwave development, as highlighted by Xue et al. (2023), are somewhat mitigated. However, the PGW approach assumes that the relationship between large-scale climate drivers and regional patterns remains constant

over time (i.e. the same climatological changes are applied every year; Brogli et al., 2023). This assumption can lead to potential misrepresentations of future MHW characteristics.

As Xue et al. (2023) point out, the effectiveness of the PGW method also depends on how perturbations (i.e. climatological changes) are applied to initial and boundary conditions. Inconsistent or inappropriate perturbations can result in significant variations in simulated outcomes, affecting the reliability of heatwave projections. Additionally, Heim et al. (2023) note that PGW is constrained by the resolution of the driving data and the capabilities of the regional model, which can impact the accurate representation of localized heatwave events. In this study, the initial and boundary conditions are derived from a coupled atmosphere–ocean Med-CORDEX regional climate model with a resolution of approximately 15 km, which is likely sufficient to capture the main dynamical properties of the Mediterranean Sea. However, the very short spin-up period (2 months) for the AdriSC RCP8.5 simulation is likely to influence the results, particularly in the first 2 to 3 years of the simulation.

Finally, by focusing on imposed large-scale changes, the PGW approach may overlook regional feedback processes, such as land–atmosphere interactions, which can influence heatwave intensity and frequency (Heim et al., 2023). A key limitation of the AdriSC climate model is that it employs a one-way coupling between the atmosphere and the ocean – i.e. the sea surface temperature from the ocean model is not fed back into the atmospheric model.

2.3 Methods

The heatwaveR package designed by Schlegel et al. (2017) and based on the MHW definitions of Hobday et al. (2016, 2018) is used to extract mean and extremum intensities, duration, cumulative heat, onset and decline intensity rates, and the starting date of each MHW event. The MHW events are defined for AdriSC daily sea surface temperatures above the daily 90th percentile (hereafter MHW threshold, illustrated in Fig. 2) for at least 5 consecutive days. As recommended in Hobday et al. (2016), the thresholds are defined over the 31-year-long historical and RCP8.5 periods, and the difference between the daily threshold and mean climatology is used to calculate the different MHW categories. Additionally, in this study, the MHW events extracted with the heatwaveR package are only selected if they cover more than 5 % of the Adriatic basin. The area of the MHW events is calculated by considering that each model grid point covers a 1 km^2 surface.

It should also be noted that, for the RCP8.5 scenario, the MHWs are extracted with the thresholds extracted from the RCP8.5 results to avoid extracting a nearly continuous MHW over the 31-year-long period of the RCP8.5 simulation (Tojčić et al., 2024). However, to simplify the comparison with the historical results, all the RCP8.5 intensities presented in this article (unless mentioned explicitly) are shifted by ΔT_{clim}, the difference between the RCP8.5 and historical daily mean climatologies (hereafter RCP8.5 MHW threshold, as illustrated in Fig. 2). This methodological adjustment is widely adopted in MHW research to enable meaningful intercomparisons across different climatological baselines (e.g. Deser et al., 2024). The rationale behind this approach is to separate the influence of background warming from the intrinsic properties of MHWs. Without such an adjustment, the intensities under RCP8.5 would reflect both the elevated baseline temperatures and the heatwave anomalies, making it difficult to isolate the climate change signal. By applying a shift equal to the difference between the RCP8.5 and historical mean climatologies, the analysis focuses on the MHWs relative to their respective mean states, thereby allowing a clearer and more direct comparison of their characteristics across time periods. Additionally, although the RCP8.5 MHW threshold exhibits pronounced seasonal variability, as shown in Fig. 2, it remains effectively constant when considering annual distributions.

All annual and monthly probability density functions of the historical and RCP8.5 intensities are normalized to have a unity area following a kernel smoothing method (Bowman and Azzalini, 1997) evaluated for 100 equally spaced points.

The category of the MHW is calculated at each grid point of the ROMS 1 km grid using the maximum intensity reached during the MHW, while the mean intensity at each model grid point is used to characterize the MHW events. For each event the cumulative heat index (CHI) is calculated by integrating the cumulative heat (i.e. mean intensity multiplied by duration) over the area of the MHW. Animations of the historical and RCP8.5 MHW events (mean intensity, duration, and category) extracted with heatwaveR over the 31 years of the simulations are presented in the Supplement (Movies S1 and S2 in Denamiel, 2025b, respectively).

For each selected MHW event and only for the grid points corresponding to the area covered by the MHW, the daily ocean vertical temperatures for the 35 sigma layers and the daily minimum and maximum air temperatures (hereafter air temperatures during night and day) are extracted from the AdriSC historical and RCP8.5 simulations. Additionally, the total air–sea net heat fluxes (Q_{net}) are calculated as described in Annex A1 of Denamiel et al. (2025). Their contribution ($\text{dSST}_{Q_{\text{net}}}$, hereafter) to the change in sea surface temperature anomaly (dSST_{A}, hereafter) during MHW onset and decline phases (between the first day and the peak of the MHW event and between the peak and the last day of the MHW event, respectively) is derived along the Adriatic coastline (between 5 and 50 m depth were most of the aquaculture is located) with the Schlegel et al. (2021) methodology previously used in the Mediterranean by Denaxa et al. (2024; see Eqs. 1 to 3). Finally, the vertically integrated ocean heat content (OHC), which corresponds to the energy absorbed by the ocean and stored as internal energy for an indefinite time period (Hansen et al., 2011; von Schuckmann et al., 2016;

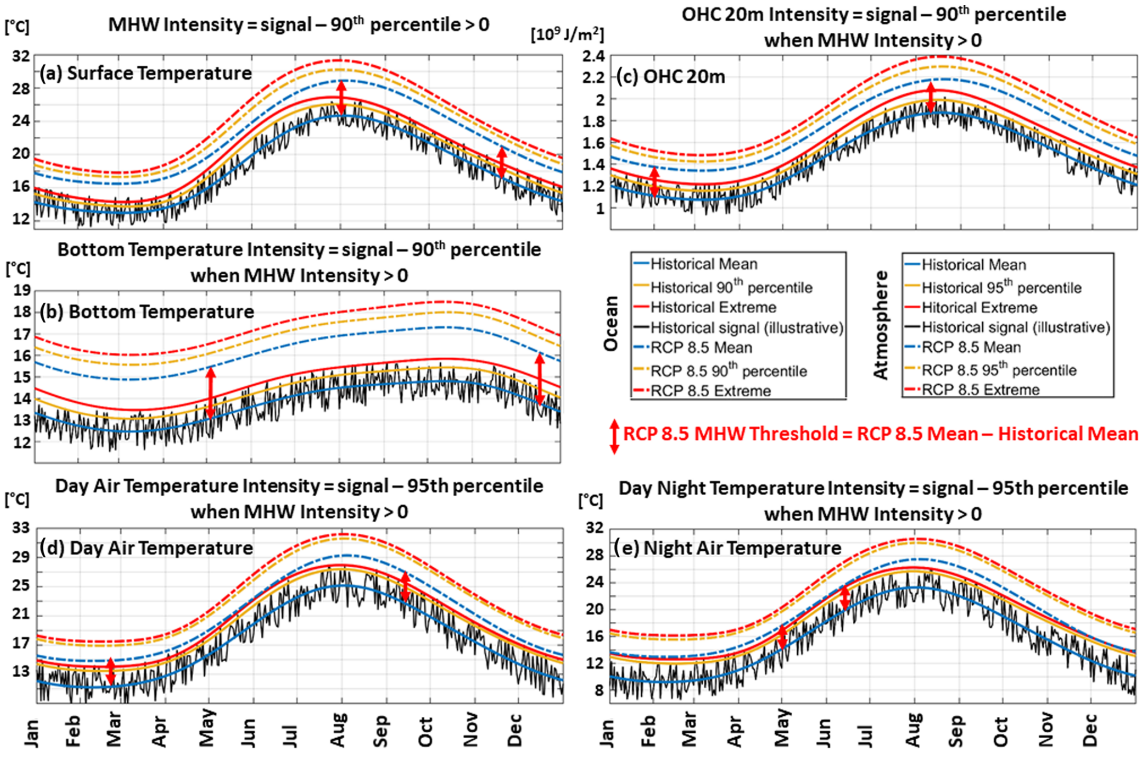

Figure 2. Illustration of the methodology used to extract the daily intensities of the sea surface temperature **(a)**, sea bottom temperature **(b)**, ocean heat content (OHC) at 20 m **(c)**, day air temperature **(d)**, and night air temperature **(e)** during the marine heatwaves (MHWs) extracted from both the historical and RCP8.5 simulations.

Trenberth et al., 2018), is computed within the upper 20 m layers.

All the other intensities are calculated by removing the daily historical 90th percentile for the ocean bottom temperatures as well as the OHCs and the daily historical 95th percentile (i.e. threshold generally used to detect daily atmospheric heatwaves; Copernicus Climate Change Service, 2023) for the air temperatures during night and day from these results and averaging them over the duration of the MHW (illustrated in Fig. 2). All thresholds are extracted from the 31-year-long period of the historical and RCP8.5 simulations.

A specific methodology has been applied for the evaluation of the influence of Adriatic Sea dynamics on MHW variability discussed in Sect. 4. Following Amaya et al. (2023) and Smith et al. (2025), both MHWs and the contributions of the total air–sea heat fluxes ($dSST_{Q_{net}}$) to the change in sea surface temperature anomaly ($dSST_A$) have been recalculated using detrended sea surface temperature signals. In this study, trends are calculated using the Theil–Sen estimation method (Mondal et al., 2012), which is robust to outliers and often more accurate than simple linear regression when applied to skewed or heteroscedastic data. This method also performs competitively with non-robust least-squares regression in terms of statistical power, even for normally distributed datasets. Additionally, the nonparametric Mann–Kendall test (originally proposed by Mann, 1945; further developed by Kendall, 1975; and Gilbert, 1987) is employed to detect the presence of monotonic (linear or nonlinear) trends by evaluating whether a time series shows a consistent increase, decrease, or no change.

For the AdriSC historical and RCP8.5 simulations, Tojčić et al. (2023, 2024) conducted a comprehensive analysis of sea surface temperature trends, variance, and extremes, showing that all identified trends are statistically significant. Notably, as illustrated in Fig. 3, the rate of surface ocean warming is 40 % higher during the historical period than under the far-future RCP8.5 scenario. Nonetheless, Tojčić et al. (2024) demonstrated that in the far-future period, the Adriatic Sea is projected to experience at least 20 additional days of extreme heat per month compared to historical conditions. This increase is primarily driven by surface temperature anomalies (i.e. differences between RCP8.5 and historical conditions) exceeding 3 °C, especially in coastal regions. Regarding sea surface temperature variance (Fig. 3b, d), an average increase of 15 % is observed across the entire Adriatic Sea, with localized increases of up to 25 % along the southeastern coastal regions. These changes further highlight the relevance of the methodology adopted to extract and analyse MHWs. For the comparison between historical and RCP8.5 conditions, the consistent climatological baseline enables the accurate identification of MHWs, while the

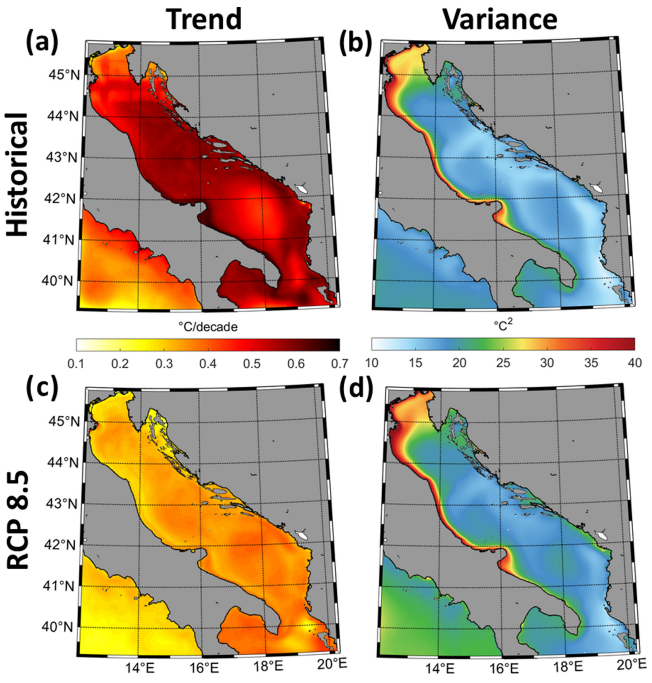

Figure 3. Trend **(a, c)** and variance **(b, d)** for the sea surface temperature over the Adriatic basin derived for the historical **(a, b)** and RCP8.5 **(c, d)** 31-year-long periods.

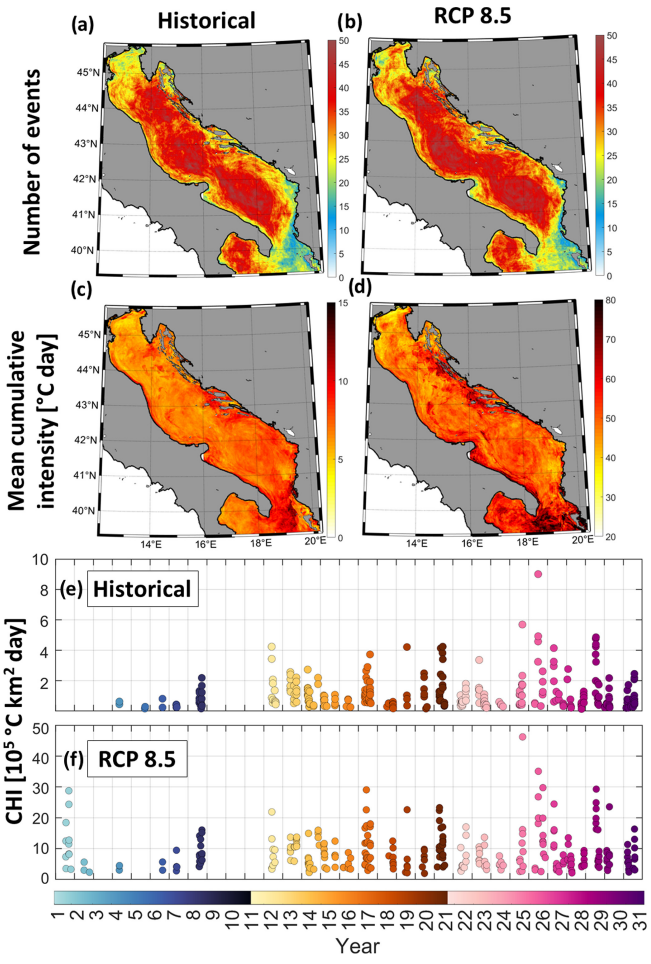

Figure 4. Spatial distributions of the total number of MHW events **(a, b)** and their associated mean cumulative intensity **(c, d)** across the Adriatic Sea for the historical period **(a, c)** and the RCP8.5 scenario **(b, d)**. Panels **(e)** and **(f)** show the time series of cumulative heat intensity (CHI) over the 31-year historical and RCP8.5 periods **(e, f)**.

additive adjustment applied to the RCP8.5 scenario helps isolate the heatwave signal from background warming. For the analysis of the influence of ocean dynamics on MHWs, the removal of the large sea surface temperature trends is necessary to properly characterize the link between dynamical features and extreme events.

Finally, as highlighted in Juza et al. (2022) and Dayan et al. (2022, 2023), subdividing the Mediterranean into subdomains is crucial to capture the high spatial variability of the ocean response to global warming and extreme events. In this study, the main advantage of using a 1 km resolution ocean model to extract MHWs is to be able to characterize the environmental conditions during these events for five different subdomains chosen for their particular dynamics. The chosen four nearshore subdomains (Fig. 1) are the northern Adriatic (NA) and the Kvarner Bay (KB) where most of the Adriatic dense water is formed, the Dalmatian Islands (DI) where a lot of tourism and fishery activities take place, and, finally, the Italian coast (IC) along the path of the Po River plume with depths below 50 m. The chosen offshore subdomain covers all the remaining Adriatic Sea areas, with depths above 50 m, including both the southern Adriatic and Jabuka pits.

3 Results

3.1 Characterization of the marine heatwave events

MHWs are first characterized over the Adriatic Sea for the 31-year period of the historical and RCP8.5 simulations through the spatial distributions of both the number of events (Fig. 4a, b) and the mean accumulative intensity (Fig. 4c, d) as well as the temporal evolution of the cumulative heat index (CHI; Fig. 4e, f). Notably, the spatial distribution of the number of MHW events remains nearly identical under both historical and far-future extreme warming conditions (RCP8.5 simulation). The deep Adriatic subdomain (Fig. 1) experiences the highest number of events (35–50), while the nearshore areas, between the coast and 50 m depth, are affected by significantly fewer events (20–35).

In terms of mean cumulative intensity, the spatial patterns under historical and far-future extreme warming conditions are also similar, with the highest and lowest values located within the Dalmatian Islands and northern Adriatic subdomains, respectively. However, a substantial increase in cumulative intensity is projected under far-future extreme warming, with values about 6 times higher (30–70 °C d) than under the historical conditions (5–12 °C d) across the entire Adriatic basin.

Regarding the CHI, historical values remain relatively low in early years (below 2×10^5 °C km^2 d for the first decade of the simulation). A gradual increase is observed over time with values exceeding 3.7×10^5 °C km^2 d (the 95th percentile of the historical distribution) and reaching up to 9×10^5 °C km^2 d in the final decade, indicating a rising trend in MHW severity.

Under far-future extreme warming conditions, CHI values are nearly an order of magnitude higher than in the historical period, consistently exceeding 10×10^5 °C km^2 d and peaking at 48×10^5 °C km^2 d in the final decade. Interestingly, unlike in the historical period, no clear increasing trend in CHI is modelled over the 31-year duration of the RCP8.5 simulation. However, the strong MHWs modelled in the first year of the RCP8.5 simulation may result from imbalances introduced by the PGW perturbations in the initial conditions. Notably, under both historical and RCP8.5 conditions, no MHWs occur during years 9–11, while the most extreme values are reached during years 25 and 26. As explained in Denamiel et al. (2025), the large-scale atmospheric and oceanographic patterns that force the boundaries of the AdriSC WRF 15 km and ROMS 3 km grids under historical conditions are also present in the RCP8.5 simulation. Consequently, the 3-year gap in MHW occurrence observed under both historical and RCP8.5 conditions is likely linked to an extraordinary atmospheric or oceanographic event, which will be further discussed in Sect. 4.

Further characterization of MHWs under historical and RCP8.5 conditions is conducted using scatter plots displaying yearly maximum values of MHW mean intensity, duration, and area (Fig. 5a, b), monthly distributions of MHW categories and event counts over the 31-year period (Fig. 5c, d), and yearly and monthly probability density distributions of MHW mean intensity (Fig. 5e). Under both historical and far-future extreme warming conditions, the yearly maximums of MHW duration are on average 40 and 46 d, respectively, the maximum affected areas mostly stay below 50 000 km^2, and the yearly maximums of mean intensity have an average of 1.7 and 5.6 °C, respectively. In both simulations, the longest-duration events (150 d) occur in year 14, while the smallest-area events (areas below 10 000 km^2) are recorded in the first 10 years. The highest maximum intensities are reached in year 25, corresponding to 2011, in the historical period and in years 1, 14, and 31 under RCP8.5.

The yearly density plots reveal that no MHWs occur in the first 3 years of the historical simulation. Initially, intensity distributions resemble Gaussian distributions, with means ranging from 0.36 to 0.57 °C during the first 10 years. Over time, they become increasingly right-skewed toward the 2 °C mark, with means between 0.35 and 0.78 °C. In contrast, under far-future extreme warming, intensity distributions are right-skewed toward 6 °C from the start of the simulation, with means ranging between 4.13 and 5.1 °C over the 31-year period. As previously noted, no MHWs are detected in years 9–11 in either simulation.

Regarding monthly heatwave categories, MHWs shift from moderate and strong in the historical period to severe and extreme under extreme warming, though their seasonal distributions remain similar, with the most extreme events occurring between May and September. The maximum number of MHW events per month (exceeding 50) occurs in August during the historical period, predominantly under strong conditions, whereas under RCP8.5, it occurs in June, primarily under severe conditions. The highest occurrences of extreme MHW conditions in the RCP8.5 scenario are recorded between July and September, coinciding with the highest occurrences of strong conditions in the historical period.

The monthly distribution of MHW intensity reveals that, on average, the most intense heatwaves occur in June under historical conditions but shift to August under far-future extreme warming. Additionally, more extreme MHW intensities (with up to a 1.2 °C increase in temperature range) are expected to occur in November and December under RCP8.5 compared to historical conditions.

Finally, the number of events per year and the distributions of the MHW mean intensity, duration, and area over the 31 years of the simulations are used to compare the results obtained under historical and RCP8.5 conditions (Fig. 6). Importantly, for consistency in comparison, the RCP8.5 mean intensities are not adjusted for the difference between RCP8.5 and historical temperature climatologies.

Notably, the AdriSC results indicate that, compared to historical conditions, MHWs under RCP8.5 conditions are significantly more intense, with median mean intensities of 0.59 and 1.14 °C and 75th percentiles of 0.80 and 1.53 °C, respectively. They also have a larger spatial extent, with median areas of about 13 000 and 15 000 km^2 and 75th percentiles of about 19 000 and 21 000 km^2, respectively. However, their duration remains similar, with median values of 8 d and 75th percentiles of 13 d under both scenarios.

Interestingly, MHWs are slightly less frequent under RCP8.5 conditions, with a total of 290 events compared to 304 events under historical conditions. This difference can be attributed to the fact that the historical trends are approximately 40 % higher than those under RCP8.5 conditions (Fig. 3) and will be further discussed in Sect. 4. Furthermore, over the last 20 years of the simulations when MHWs occur annually, the correlations between median yearly variations in MHW intensity, area, and duration under historical and RCP8.5 conditions reach 0.92, 0.44, and 0.91, respectively. These high correlations between historical and

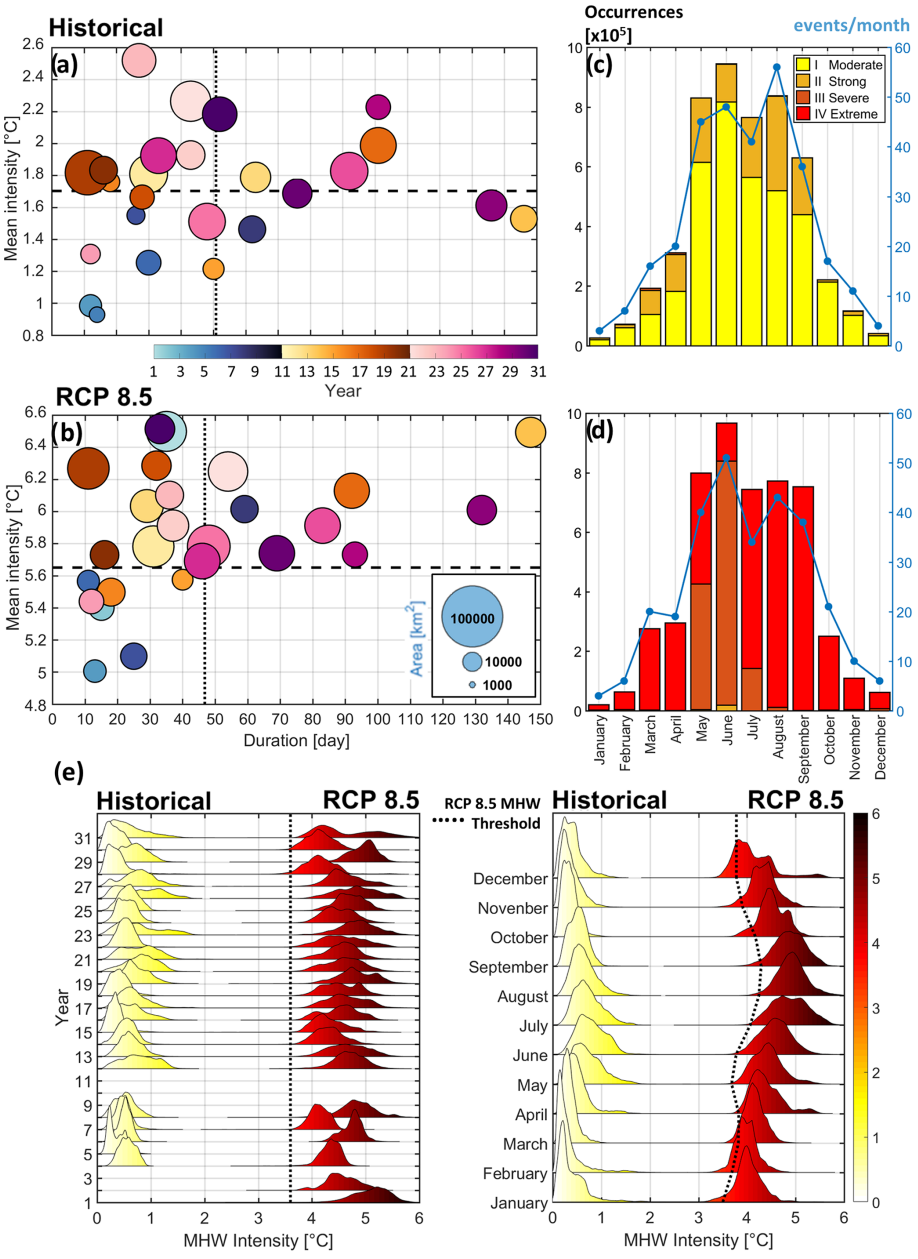

Figure 5. Scatter plots of the yearly maximum value of the MHW mean intensity versus the maximum yearly value of the duration of the MHW with the size of the circles depending on the maximum yearly value of the area covered by the MHW during the historical **(a)** and RCP8.5 **(b)** 31-year-long periods. Monthly distributions of both the MHW categories – with each occurrence representing one cell of the model – presented as histograms and the number of MHW events during the historical **(c)** and RCP8.5 **(d)** 31-year-long periods. Yearly (left) and monthly (right) probability density distributions of the MHW mean intensity during the historical and RCP8.5 31-year-long periods **(e)**. All probability density distributions are normalized to unit area to facilitate direct comparison.

RCP8.5 MHW intensity, area, and duration are likely a consequence of the PGW approach – which assumes that the relationship between large-scale climate drivers and regional weather patterns remains constant over time – rather than realistic temporal features.

3.2 Environmental conditions during the marine heatwave events

The environmental conditions during historical and RCP8.5 MHWs are analysed across five subdomains: northern Adriatic, Kvarner Bay, Italian coast, Dalmatian Islands, and deep Adriatic (Fig. 1). These conditions are presented as overall

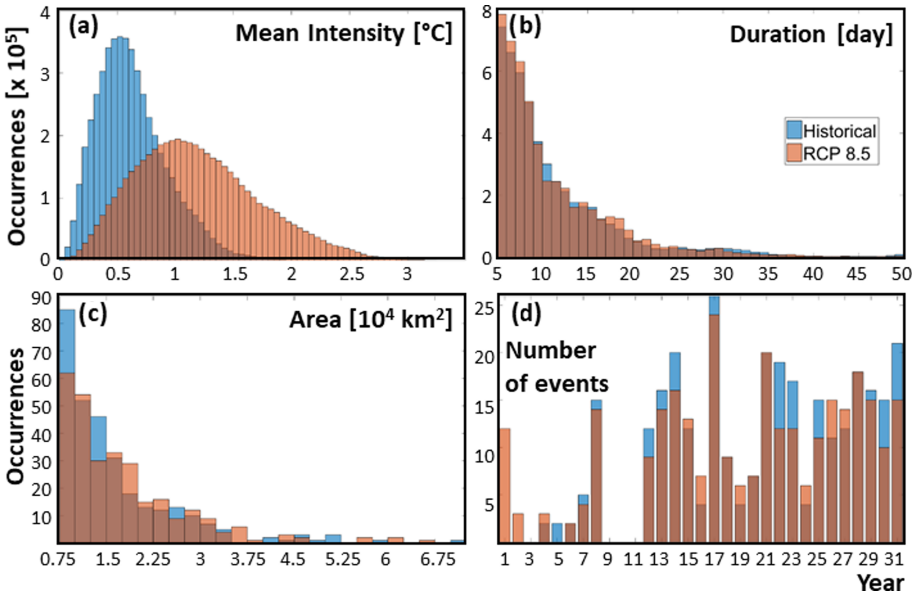

Figure 6. Distributions of the MHW mean intensity as originally extracted with the heatwaveR package **(a)**, duration **(b)**, and area **(c)** as well as yearly time series of the number of MHW events defined over the 31 years for the historical and RCP8.5 conditions.

distributions and monthly climatologies of the median and 25th and 75th percentiles for MHW intensity, bottom temperature, and ocean heat content (OHC) at 20 m depth in the ocean (Fig. 7), as well as for day and night air temperature intensities in the atmosphere (Fig. 8).

Regarding the distributions of MHW mean intensities under historical conditions, median and 75th percentile values are approximately 0.60 and 0.80 °C for the northern Adriatic (0.60, 0.80 °C), Kvarner Bay (0.62, 0.86 °C), Dalmatian Islands (0.58, 0.80 °C), and deep Adriatic (0.57, 0.79 °C) subdomains. In contrast, the Italian coast subdomain shows lower values, at 0.53 and 0.71 °C, respectively. Under the RCP8.5 scenario, median and 75th percentile values increase significantly, ranging from 4.37 and 4.62 °C in the northern Adriatic to 4.70 and 5.00 °C in the deep Adriatic. The proportion of occurrences above heatwave thresholds is derived from the distributions of bottom temperature, OHC at 20 m, and day and night air temperature intensities (Table 1). Results show that, during historical surface MHW events, 28 %–32 % of bottom ocean temperatures and 45 %–54 % of OHC at 20 m exceed their heatwave thresholds in the northern Adriatic, Kvarner Bay, Dalmatian Islands, and deep Adriatic subdomains. However, in the Italian coast subdomain, these proportions are significantly higher, with 42 % of bottom ocean temperatures and 62 % of OHC at 20 m exceeding their thresholds.

For RCP8.5 surface MHW events, only 20 %–23 % of bottom temperatures exceed their thresholds in the Kvarner Bay and Dalmatian Islands subdomains, while proportions remain similar to historical conditions for the other subdomains. In contrast, the proportion of OHC at 20 m exceeding its threshold increases under RCP8.5 compared to historical conditions, particularly in Kvarner Bay (60 % vs. 54 %), Dalmatian Islands (65 % vs. 45 %), and the deep Adriatic (51 % vs. 47 %). Additionally, across all subdomains, a higher percentage of night and day air temperatures exceed their thresholds under RCP8.5 (37 %–44 % and 43 %–50 %, respectively) compared to historical conditions (28 %–37 % and 32 %–44 %, respectively). Notably, the presence of a double peak in the distribution of ocean bottom temperature intensities in the deep Adriatic subdomain (at about 0.5 and 3 °C; Fig. 7b) is linked to the fact that, under the RCP8.5 scenario, the shallow areas of the Adriatic Sea are expected to warm by up to 3.5 °C, while the deepest parts are expected to warm only by up to 0.5 °C (Denamiel et al., 2025). Consequently, as the ocean bottom temperature threshold is defined for all depths within the deep Adriatic subdomain, which has an average depth of approximately 300 m, no definitive conclusions about bottom MHWs can be drawn for the deepest part of the Adriatic Sea (southern Adriatic Pit; Fig. 1). This also explains the 2 °C spread (between the 25th and 75th percentiles) of the bottom temperatures seen in the monthly climatology within the deep Adriatic subdomain.

In terms of the monthly climatologies, for all the subdomains, most of the MHW mean intensities vary between 0.25 and 1 °C under the historical conditions and between 3.5 and 5 °C for the RCP8.5 scenario, with the highest values reached between April and September. However, for the Italian coast and northern Adriatic subdomains, the highest MHW intensities are also reached in December and January, particularly under the historical conditions. The monthly climatologies of both bottom temperature and OHC at 20 m present similar

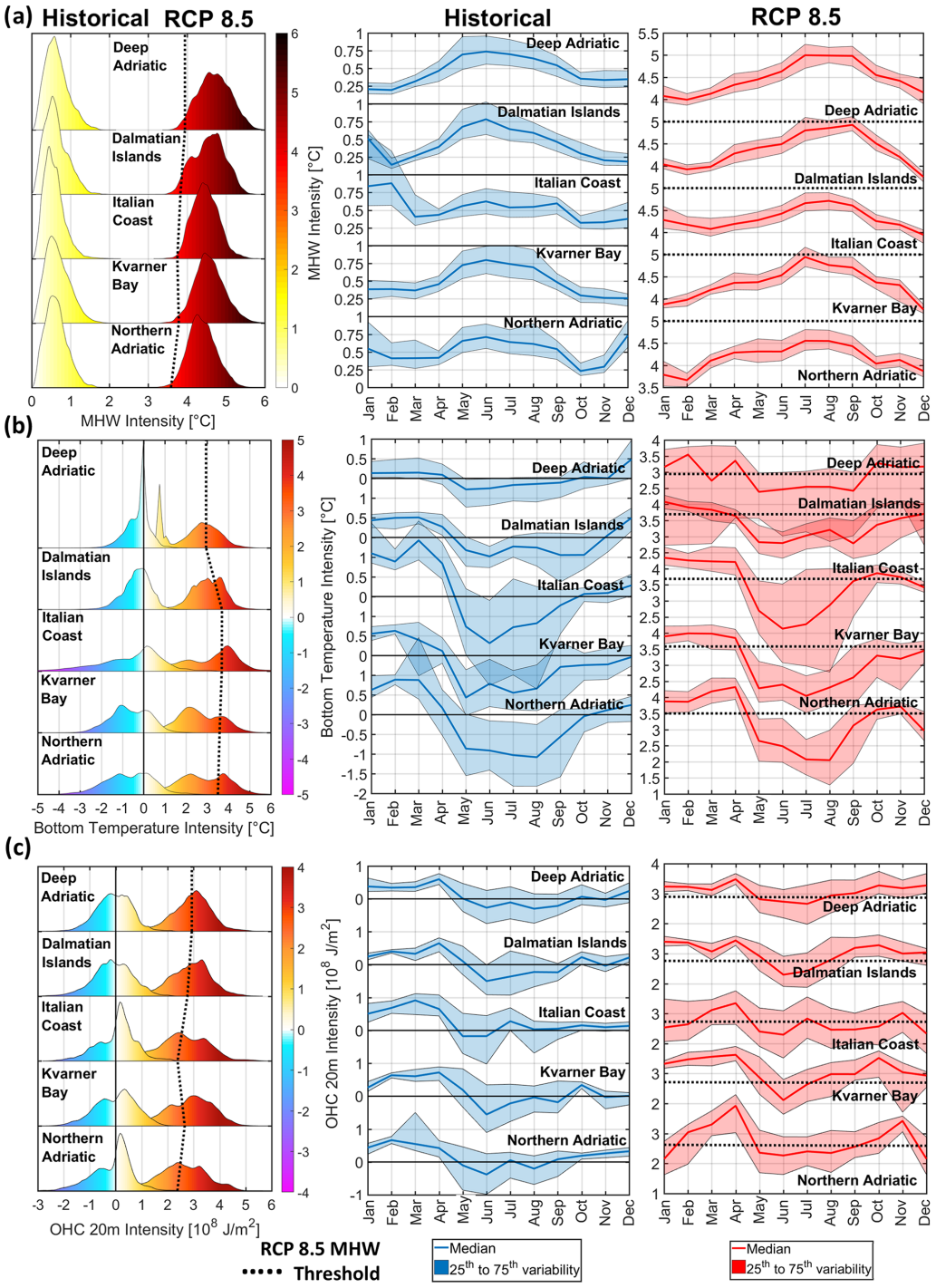

Figure 7. For the five selected subdomains (northern Adriatic, Kvarner Bay, Italian coast, Dalmatian Islands, and deep Adriatic), distributions (left panels) and monthly climatologies of the median and 25th and 75th percentiles (centre and right panels) of the MHW **(a)**, ocean bottom temperature **(b)**, and OHC at 20 m **(c)** intensities defined over the 31 years for the historical and RCP8.5 conditions. All probability density distributions are normalized to unit area to facilitate direct comparison.

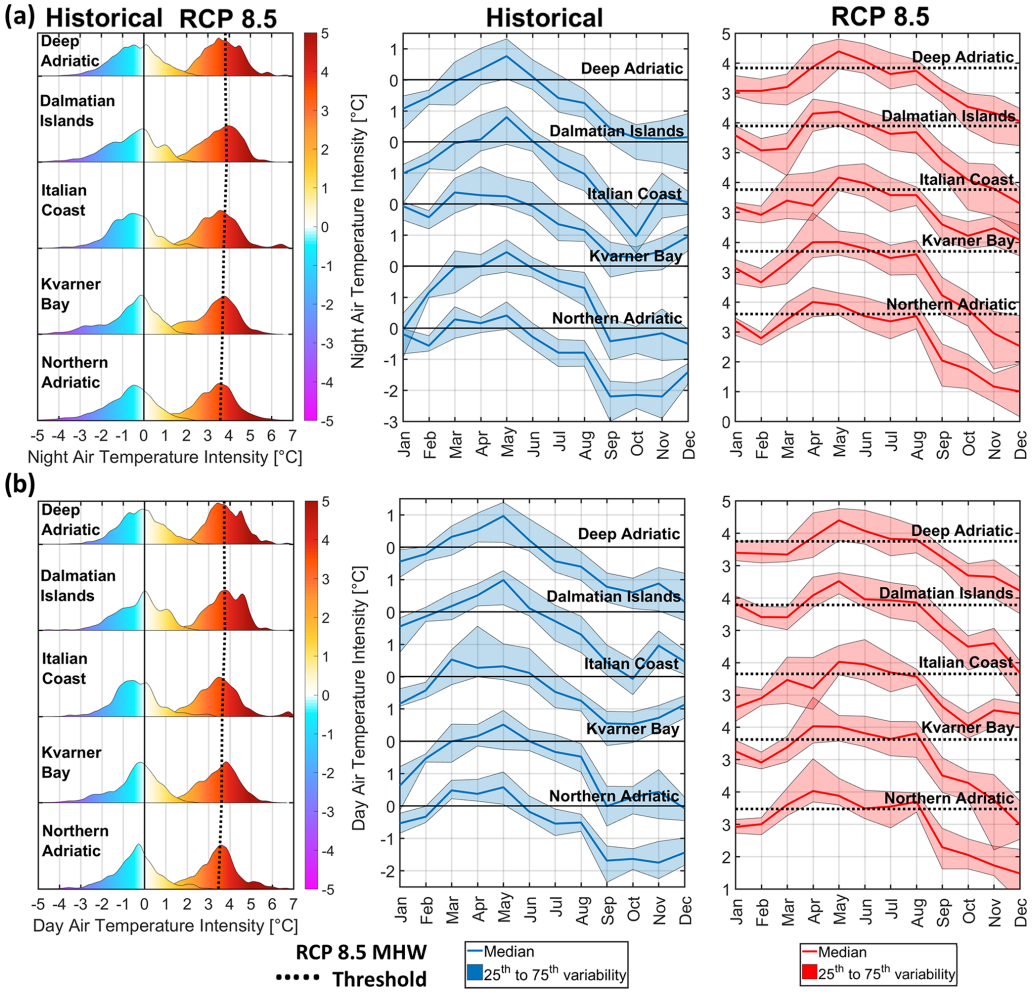

Figure 8. For the five selected subdomains (northern Adriatic, Kvarner Bay, Italian coast, Dalmatian Islands, and deep Adriatic), annual distributions (left panels) and monthly climatologies of the median and 25th and 75th percentiles (centre and right panels) of the night **(a)** and day **(b)** air temperature intensities defined over the 31 years for the historical and RCP8.5 conditions. All probability density distributions are normalized to unit area to facilitate direct comparison.

Table 1. Proportion (in percent) of occurrences of historical and RCP8.5 bottom ocean temperature, OHC at 20 m, and night and day air temperatures above the historical and RCP8.5 thresholds, respectively.

	Bottom ocean temperatures		OHC at 20 m		Night air temperatures		Day air temperatures	
	Historical	RCP8.5	Historical	RCP8.5	Historical	RCP8.5	Historical	RCP8.5
Northern Adriatic	30 %	32 %	54 %	51 %	28 %	40 %	32 %	48 %
Kvarner Bay	28 %	23 %	54 %	60 %	33 %	40 %	37 %	48 %
Italian coast	42 %	43 %	62 %	57 %	29 %	37 %	32 %	43 %
Dalmatian Islands	32 %	20 %	45 %	65 %	34 %	39 %	44 %	52 %
Deep Adriatic	32 %	32 %	47 %	51 %	37 %	44 %	43 %	50 %

variations for all the subdomains. Under the historical conditions, they exceed their threshold – i.e. their extremes coincide with surface MHWs – mostly in winter between November and April. Under the RCP8.5 conditions, in the northern Adriatic and Italian coast subdomains, bottom temperatures and OHC at 20 m experience the impact of surface MHWs between February and May as well as between September and November but tend to be below their thresholds in December and/or January. Further, the Italian coast subdomain presents the largest variations in bottom temperature intensities (more than 2.5 °C) during summer between May and September. However, in the Kvarner Bay, Dalmatian Islands, and deep Adriatic subdomains, the OHC at 20 m thresholds are surpassed between July and May, which means that surface MHWs influenced the first 20 m of these domains most of year. Additionally, in the Kvarner Bay and Dalmatian Islands subdomains, the bottom temperatures only surpass their threshold between January and April under both historical and RCP8.5 conditions. In contrast with the ocean results, for all the subdomains, the night and day air temperature intensities mostly exceed their thresholds between March and July for both historical and RCP8.5 conditions. Consequently, atmospheric heatwaves are more likely to occur during MHWs in spring and summer.

In order to further explore the connection between MHWs and atmospheric conditions under both historical and RCP8.5 conditions, the contribution of total air–sea heat fluxes ($dSST_{Q_{net}}$) to the change in sea surface temperature anomaly ($dSST_A$) is examined during the onset and decline of the MHWs. The results are presented as distributions over the entire Adriatic Sea (Fig. 9a), percentage of air–sea-driven events within the four coastal subdomains (Dalmatian Islands, Kvarner Bay, northern Adriatic and Italian coast; Fig. 9b), and distributions of the events depending on the depth and location of the subdomains (Fig. 10). Importantly, the percentage of events primarily driven by air–sea heat fluxes is calculated under the assumption that the contribution of total air–sea heat fluxes to the change in sea surface temperature anomaly is considered significant when more than half of the warming/cooling can be attributed to air–sea heat fluxes – i.e. $dSST_{Q_{net}}/dSST_A > 0.5$.

Under this assumption, MHWs are predominantly influenced by the air–sea fluxes during their onset phase compare to their decline for all subdomains and both scenarios. Furthermore, under both historical and RCP8.5 scenarios, air–sea fluxes exert the strongest influence on MHWs within the northern Adriatic (24 % and 28 %) and Italian coast (34 % and 40 %) subdomains, while their impact is weaker in the Dalmatian Islands (20 % and 25 %) and Kvarner Bay (18 % and 23 %) subdomains.

Finally, as shown in Fig. 10, air–sea fluxes tend to influence both the onset and decline of nearshore MHWs (i.e. at depths between 5 and 20 m), particularly within the northern Adriatic and Italian coast subdomains. Under historical conditions, the distributions of air–sea influence during the onset and decline phases appear symmetrical, indicating that air–sea fluxes primarily impact the onset of MHWs. However, under RCP8.5 conditions, this symmetry is lost, with an increasing number of events influenced by air–sea fluxes during the decline phase of MHWs.

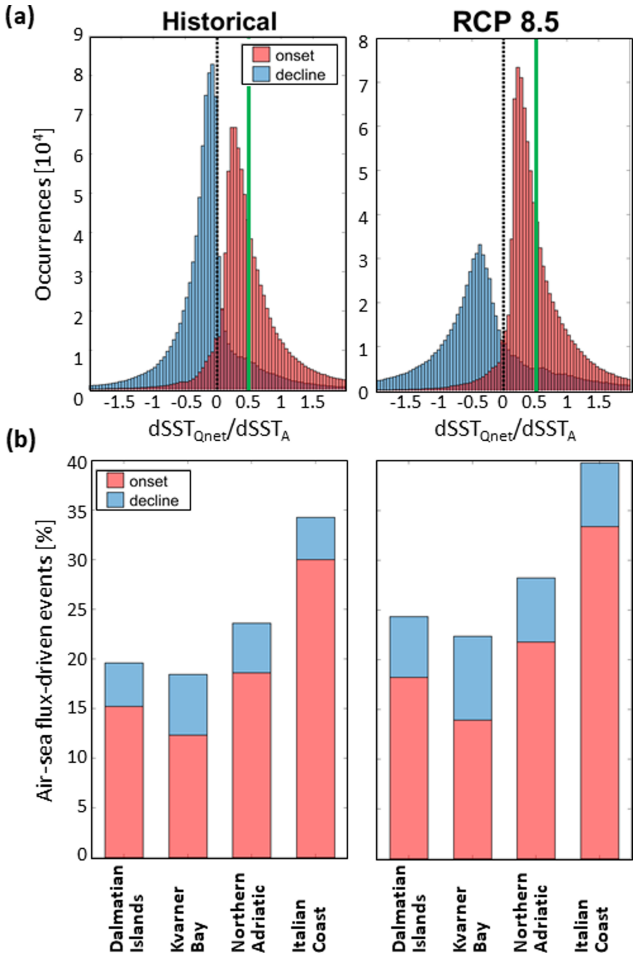

Figure 9. Contribution of total air–sea heat fluxes ($dSST_{Q_{net}}$) to the change in sea surface temperature anomaly ($dSST_A$) during MHW onset and decline phases along the nearshore areas of the Adriatic Sea (between 5 and 50 m depth) over the 31-year period of the historical and RCP8.5 simulations **(a)**. Percentage of events primarily driven by air–sea heat fluxes (i.e. with more than half of the warming/cooling attributed to air–sea heat fluxes) for the four nearshore subdomains **(b)**.

4 Discussion

4.1 Performance of the AdriSC model

In terms of the capacity of the AdriSC model to reproduce historical MHW events, the strongest MHWs extracted above the 95th percentile of the AdriSC cumulative heat index results ($CHI \geq 3.7\,°C\,km^2\,d$; Fig. 4e) – corresponding to the

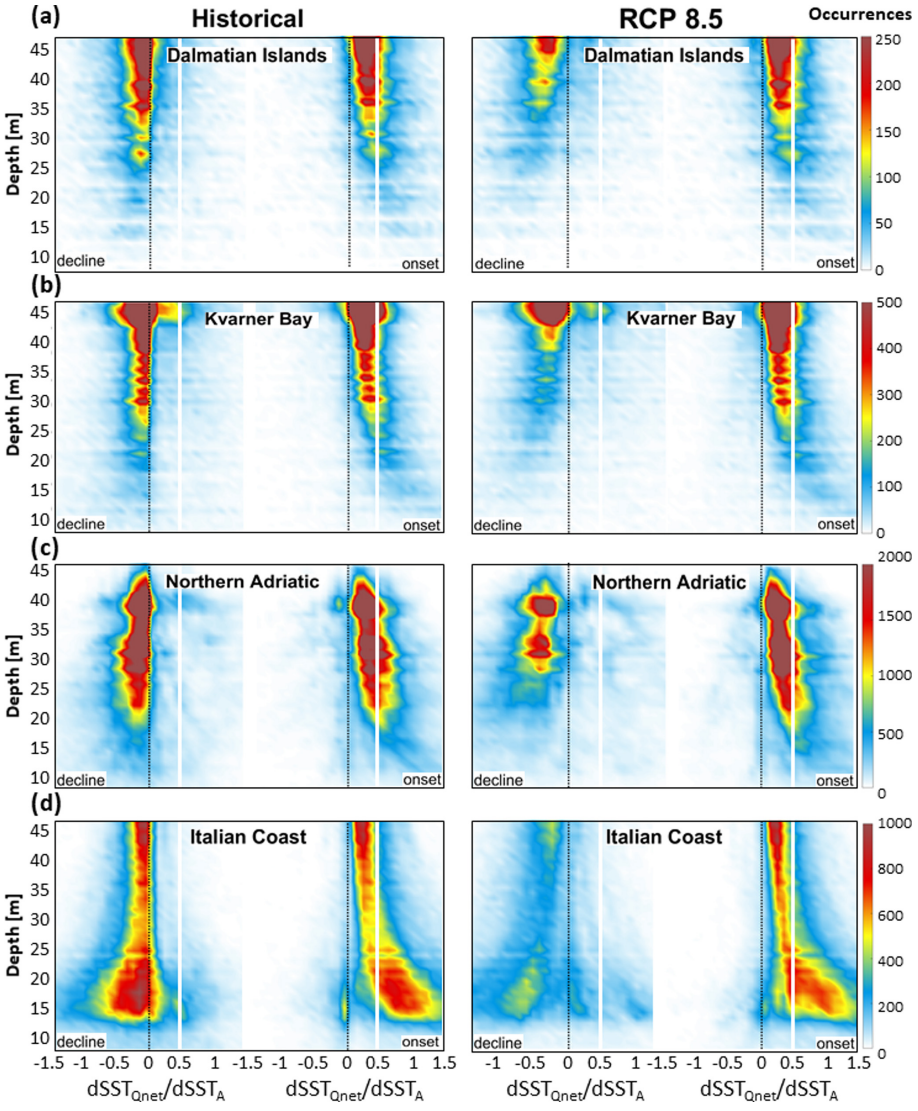

Figure 10. Distribution of the contribution of total air–sea heat fluxes (dSST$_{Q_{net}}$) to the change in sea surface temperature anomaly (dSST$_A$) during MHW onset and decline phases depending on the depths (between 5 and 50 m) of the four nearshore subdomains and over the 31-year-long periods of the historical and RCP8.5 simulations.

years 1998, 2003, 2005, 2007, 2009, 2011, 2012, 2013, and 2015 – can be confirmed by several observational studies. For instance, Sparnocchia et al. (2006) documented an extreme MHW during the summer of 2003 using in situ observations in the central Ligurian Sea, noting record-high sea surface temperature anomalies that align with the AdriSC detection of 2003 as one of the longest and strongest Adriatic events. In a recent study, Martínez et al. (2023) analysed long-term sea surface temperature (SST) records in the Mediterranean and identified significant MHW occurrences in 1998, 2003, 2007, 2012, and 2015, emphasizing the interannual variability of these events. It should be noted that Martínez et al. (2023) identified more Adriatic MHWs than the AdriSC model in the first half of the 1987–2017 period as they used detrended sea surface temperature data. In the Adriatic, Salini et al. (2024) analysed the heatwaves along the Italian Adriatic coast between 2008 and 2022. They found that the 2009 MHW was the most intense event, with more than 4 °C of anomaly peak intensity, while the 2011 MHW was more intense in the northern Adriatic. Moreover, Garrabou et al. (2019) linked recurrent marine heatwaves across the Mediterranean to ecological impacts, noting substantial events during 2005, 2012, 2013, and 2015. This convergence of evidence suggests that the years flagged by the AdriSC model are consistent with observational studies.

Furthermore, the AdriSC results, showing that historical MHWs occurring in winter (from November to March) are more likely to affect the temperatures of the entire water col-

umn than summer events, are partially confirmed by the studies by Olita et al. (2007) and Garrabou et al. (2009). These studies demonstrated that the exceptional Mediterranean MHW in 2003 led to elevated sea temperatures during both summer and winter months that contributed to widespread mortality across various marine species including rocky benthic communities. Merryfield (2000) and Radko et al. (2014) have also demonstrated that, during summer, the Mediterranean Sea and, hence, the Adriatic Sea experience strong thermal stratification, characterized by a warm, less dense surface layer overlying cooler, denser deep waters which inhibits vertical mixing, confining MHW effects on the surface layers. In winter, surface cooling and increased wind activity reduce stratification, promoting vertical mixing, which allows MHWs to penetrate deeper into the water column, affecting subsurface and benthic ecosystems.

Concerning the projection of MHW events under extreme far-future warming, global studies project an increase in MHW intensity by up to approximately 50 % relative to historical values, while the duration of these events may double (Smale et al., 2019; Perkins-Kirkpatrick and Lewis, 2020). Further, the study of Konsta et al. (2025) – based on a global climate model with a horizontal resolution of about 11 km and using shifted baseline climatologies (similar to the presented study) – indicates that continued warming under RCP8.5 could lead to shorter and milder shallow MHWs within the Mediterranean marine protected areas including the Adriatic Sea. In contrast, the AdriSC results based on the PGW methodology suggest that under extreme far-future warming, Adriatic MHWs are likely to intensify and have a larger spatial extent, while their duration will remain identical to the historical conditions and their frequency will slightly decrease. However, region-specific studies focusing solely on the Adriatic Sea remain limited.

Finally, during the summer season, under both historical and far-future extreme warming, the deep Adriatic, Dalmatian Islands, and Kvarner Bay subdomains are found to experience the strongest MHWs (Fig. 7a), which is confirmed by both observations and an ensemble of models in the study of Bonaldo et al. (2025). As highlighted by Glamuzinaet al. (2024) the extreme warming already experienced in the eastern Adriatic Sea leads to higher risk of invasiveness of non-native marine organisms. This increased invasiveness poses threats to native biodiversity and can disrupt existing fisheries and aquaculture operations. Additionally, extreme temperature events can cause mass mortality in marine species. For example, a significant die-off of Mediterranean mussels along the middle Adriatic coast already happened in summer 2022 and was linked to the effects of climate change, highlighting the vulnerability of aquaculture operations to MHWs (Bracchetti et al., 2024).

4.2 Added value of the pseudo-global-warming method

In the preceding sections, MHWs were identified using an updated reference period for the RCP8.5 scenario (Smith et al., 2025), which represents a standard approach when employing the PGW methodology. In this subsection, MHWs are instead extracted using a detrended baseline following Smith et al. (2025) in order to better isolate and evaluate the influence of oceanic dynamics on the characteristics of MHWs.

4.2.1 MHW characteristics under the detrended baseline

The MHWs identified using the detrended baseline framework are first characterized by the number of events per year, along with the distributions of their mean intensity, duration, and spatial extent over the 31-year historical and RCP8.5 simulations (Fig. 11a–d). Importantly, for consistency in comparison, the RCP8.5 mean intensities are not adjusted to account for the difference between the RCP8.5 and historical temperature climatologies.

In contrast to the previous results, the intensities of MHWs under historical and RCP8.5 conditions are comparable, with median mean intensities of 0.59 and 0.63 °C and 75th percentiles of 0.80 and 0.87 °C, respectively. Their spatial extent is also similar, with median areas of approximately 13 800 km^2 and 13 600 km^2 and 75th percentiles of about 20 400 and 21 400 km^2, respectively. However, as in the previous results, their duration remains consistent, with median values of 8 d and 75th percentiles of 12–13 d.

Additionally, in contrast with the previous results, within the detrended baseline framework, MHWs are slightly more frequent under RCP8.5 conditions, with a total of 287 events compared to 280 events under historical conditions. Notably, during the first 8 years of the historical and RCP8.5 simulations, the number of MHW events increases significantly under this framework – reaching 117 and 91 events, respectively, compared to just 26 and 38 events, respectively, in the previous (non-detrended) results. These results clearly highlight the influence of long-term temperature trends on the detection and characterization of marine heatwaves. In particular, the significant increase in the number of events during the early years of both simulations under the detrended baseline framework – compared to the original results – demonstrates that background warming trends in the Adriatic Sea can obscure or delay the identification of MHWs. By removing these trends, it becomes possible to isolate the intrinsic variability and short-term anomalies that define MHW events, thus offering a more consistent basis for defining the impact of the ocean dynamics on the MHWs.

Further characterization of MHWs under historical and RCP8.5 conditions is carried out using yearly probability density distributions of MHW mean intensity (Fig. 11e) and scatter plots displaying the yearly maximum values of MHW

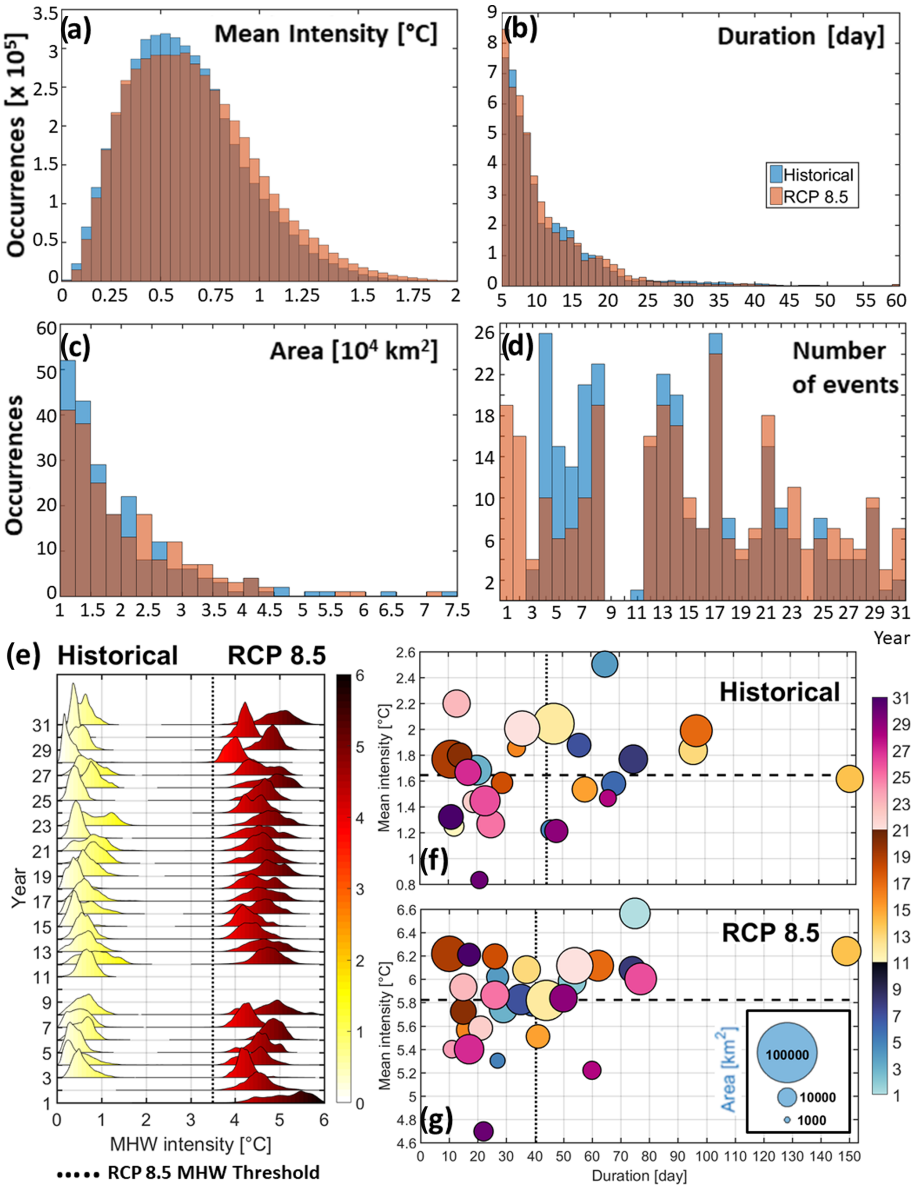

Figure 11. MHW characteristics based on the detrended sea surface temperature. Distributions of the mean intensity as originally extracted with the heatwaveR package **(a)**, duration **(b)**, and area **(c)** as well as yearly time series of the number of events defined over the 31 years for the historical and RCP8.5 conditions. Yearly probability density distributions of the mean intensity during the historical and RCP8.5 31-year-long periods **(e)**. All probability density distributions are normalized to unit area to facilitate direct comparison. Scatter plots of the yearly maximum value of the mean intensity versus the maximum yearly value of the duration, with the size of the circles depending on the maximum yearly value of the area during the historical **(f)** and RCP8.5 **(g)** 31-year-long periods.

mean intensity, duration, and spatial extent (Fig. 11f, g). The density plots reveal that, under historical conditions, no MHWs are detected in the first 2 years of the simulation – compared to the first 3 years in the previous (non-detrended) results. As in the previous analysis, no MHWs are identified in years 9–10 in either simulation; however, in year 11, one event is detected under historical conditions (Fig. 11d). Under both historical and far-future extreme warming scenarios, the yearly maximum MHW durations (on average 42 and 40 d, respectively), maximum mean intensities (on average 1.6 and 5.6 °C, respectively), and maximum affected areas (mostly below 50 000 km^2) remain comparable to those obtained with the non-detrended baseline. The most notable difference between the two approaches lies in the increased detection of more intense and longer MHWs during the first decade of both simulations when using the detrended baseline, again highlighting the impact of baseline trends on the timing and characteristics of MHW detection.

Overall, the comparison between detrended and non-detrended baselines underscores how baseline selection influences the interpretation of marine heatwave characteristics. While the non-detrended approach captures the compounded effects of long-term warming and short-term variability, the detrended baseline isolates interannual to decadal variability more effectively. This distinction provides complementary insights: the former emphasizes the trajectory of change under climate forcing, while the latter enhances the detection of underlying oceanic dynamics. Together, these methodologies offer a more comprehensive understanding of future MHW behaviour in a rapidly warming Adriatic context.

4.2.2 Impact of the Po River plume

For both historical and RCP8.5 scenarios, the results presented in this study clearly highlight that the northern Adriatic and Italian coast subdomains exhibit seasonal variations in bottom temperature and ocean heat content (OHC) at 20 m that differ significantly from the rest of the Adriatic Sea. These regions also experience the strongest influence of air–sea fluxes on sea surface temperatures, particularly during the onset phase of MHWs.

In these areas, freshwater discharge from the Po River generates a buoyant plume that induces stratification, which, as noted by Verri et al. (2024), can act as a barrier to vertical mixing. This process potentially traps heat in the surface layers, contributing to elevated sea surface temperatures. Conversely, during periods of reduced river discharge, weaker stratification may enhance vertical mixing, redistributing heat more evenly throughout the water column and potentially mitigating surface warming. Additionally, Pranić et al. (2021) highlight that the Po River plume carries suspended sediments and organic matter, altering the optical properties of northern Adriatic waters. These changes can influence the absorption of solar radiation, thereby affecting sea surface temperatures. Areas with higher turbidity due to the plume may experience reduced solar penetration, leading to cooler surface waters, while clearer waters may allow for deeper solar penetration, affecting the thermal structure and potentially influencing the development and intensity of MHWs. Furthermore, the Po River discharge exhibits seasonal variability, with peak flows typically occurring in late autumn and spring and lower flows in winter and summer.

Sani et al. (2024) demonstrate that this variability influences circulation patterns in the northern Adriatic Sea, affecting the distribution of water masses and heat content. During periods of high discharge, the expanded plume can modify local currents and stratification, potentially impacting the onset and duration of MHWs.

In the AdriSC historical simulation, the Po River discharge is modelled using historical observations, which indicate the lowest discharges (below $1000\,m^3\,s^{-1}$) in January–March and August–September and the highest (above $1500\,m^3\,s^{-1}$) in May–June and November. Under the PGW approach used in the AdriSC RCP8.5 simulation, historical discharges are increased by approximately 15 % between September and December and up to 50 % in January and February, while decreasing by up to 50 % between March and August – see Pranić et al. (2021) for more details. As a result, under RCP8.5 conditions, the lowest discharges (below $1000\,m^3\,s^{-1}$) occur in March–April and June–September, while the highest discharges (above $1500\,m^3\,s^{-1}$) occur in October–November. Additionally, the temperature of the Po River plume is based on ground air temperature extracted from the ERA-Interim reanalysis near the delta, modified using the PGW approach for the RCP8.5 scenario. The optical properties of the waters along the Po River plume remain identical under historical and RCP8.5 conditions and have been corrected to better represent historical conditions.

After recalculation of the MHWs with the detrended sea surface temperature signal, the AdriSC model results (Fig. 12) do not align with the conclusions of Verri et al. (2024). First, under historical conditions, no or weak correlations are found in the northern Adriatic (0.11) and along the Italian coast (0.05) between monthly MHW intensities and Po River discharge. However, between August and April, anticorrelations reach -0.54 in the northern Adriatic and -0.71 along the Italian coast. Additionally, under far-future extreme warming, the anticorrelations reach -0.49 in the northern Adriatic and -0.51 along the Italian coast. Second, as shown in Fig. 12, for both the northern Adriatic and Italian coast subdomains, no correlation is found between the Po River discharge and $dSST_{Q_{net}}/dSST_A$ during the MHW onset under historical conditions, while anticorrelations of approximately -0.5 are observed under the RCP8.5 scenario. However, under historical conditions, between August and April, the anticorrelations reach -0.45 in the northern Adriatic and -0.21 along the Italian coast. For the decline of MHWs, positive correlations are observed: 0.13 and 0.66 in the northern Adriatic and 0.14 and 0.58 along the Italian coast for historical and RCP8.5 conditions, respectively. However, between August and April, these correlations increase to 0.71 in the northern Adriatic and 0.56 along the Italian coast under historical conditions.

In summary, lower Po River discharge is more likely to coincide with the onset of intense MHWs, whereas higher discharges are associated with their decline. This relationship is mostly driven by air–sea fluxes between August and April under historical conditions but persists year-round under far-future extreme warming. Furthermore, these MHWs extend to the bottom of the Adriatic Sea along the Po River plume between August and April under historical conditions, as well as from February to May and September to November under the RCP8.5 scenario (Fig. 7, northern Adriatic and Italian coast subdomains).

These findings using the PGW approach suggest that MHWs are more likely to develop and persist under low Po River discharge conditions, when water clarity increases and

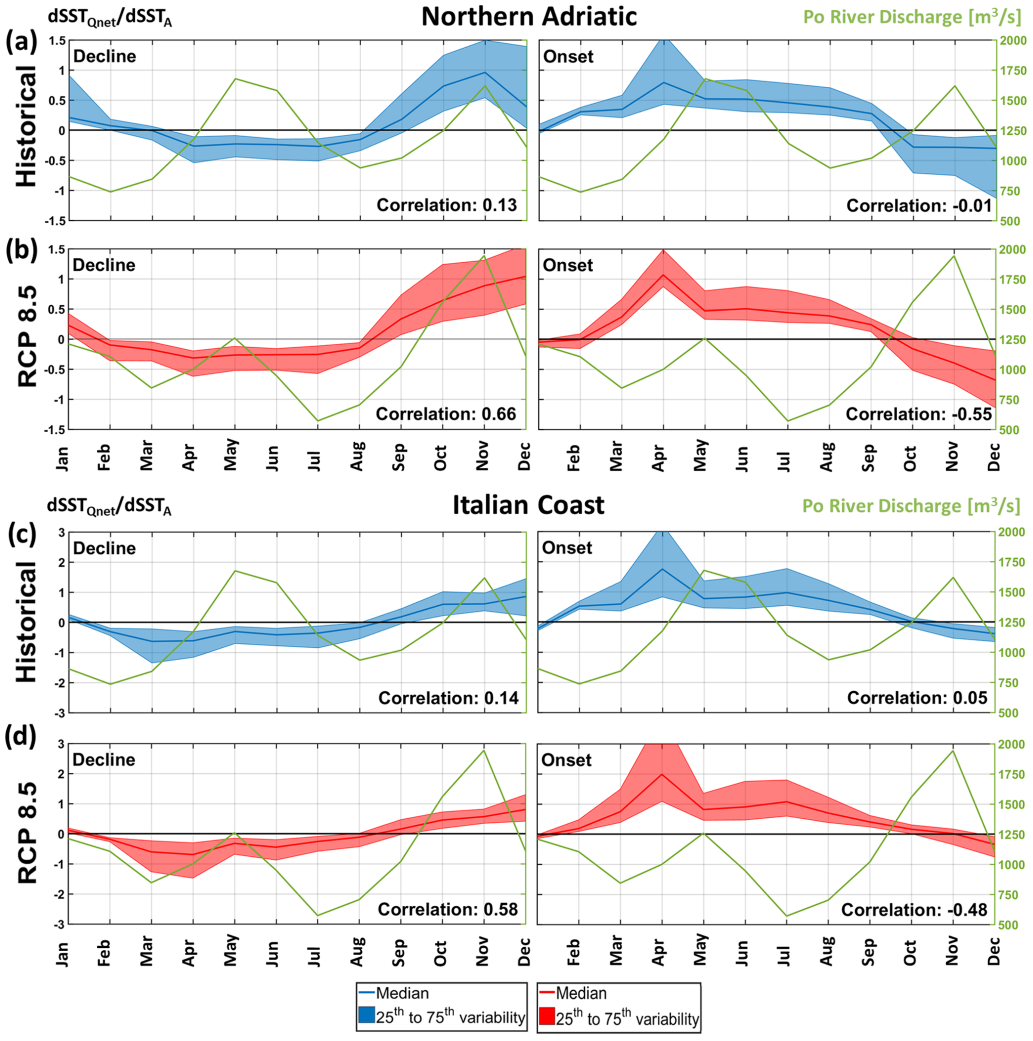

Figure 12. For the northern Adriatic **(a, b)** and Italian coast **(c, d)** subdomains, monthly climatologies of the median and 25th and 75th percentiles of the contribution of total air–sea heat fluxes (dSST$_{Q_{net}}$) to the change in sea surface temperature anomaly (dSST$_A$) during MHW onset and decline phases with the monthly climatology of the Po River discharge superimposed (in green) and defined over the 31 years for the historical (**b, d**, in blue) and RCP8.5 (**a, c**, in red) conditions.

solar radiation absorption is enhanced due to reduced suspended sediments and organic matter. Additionally, the temperature of the Po River plume may influence MHW occurrence, particularly during summer, when (anti)correlations are weak, especially under historical conditions. In particular, the trends and variance of sea surface temperatures calculated over the Adriatic Sea for the 31-year historical and RCP8.5 periods (Fig. 3) reveal the influence of the Po River. Specifically, under both historical and RCP8.5 conditions, a distinct pattern emerges along the path of the Po River plume in the northern Adriatic. Compared to other shallow areas of the basin, this region exhibits a slower rate of warming (0.45 vs. 0.7 °C per decade under historical conditions and 0.2 vs. 0.35 °C per decade under RCP8.5), coupled with markedly higher variance in sea surface temperature (up to 40 vs. 20 °C^2). These results highlight the significant role of riverine influence in modulating local climate signals. Therefore, accurately representing Po River dynamics – including its temperature, suspended sediments, and organic matter – is crucial for predicting the impacts of climate change on MHW frequency and intensity in the Adriatic Sea.

4.2.3 Impact of significant oceanographic events

One of the most interesting features of the MHW results presented in this study is that, for both historical and far-future extreme warming conditions, no MHW is detected during years 9 to 11. After recalculating the MHWs using the detrended sea surface temperature signal, this result is largely confirmed, except for the presence of a very weak MHW in year 11 under historical conditions (Figs. 11d, e and 13; CHI variability). In the historical simulation, this

period corresponds to the Eastern Mediterranean Transient (EMT) event, which is characterized by massive dense water formation triggered by extreme heat losses and high salinity in the Aegean Sea during winter 1992–1993 (Roether et al., 1996, 2007; Klein et al., 1999; Velaoras et al., 2017). During the EMT, the northern Ionian Sea is filled with very dense water from the Aegean Sea, and the intrusion of Adriatic-originated water into the Levantine basin is blocked (Akpinar et al., 2016; Li and Tanhua, 2020). As explained in Denamiel et al. (2025), the RCP8.5 scenario presented in this study is also forced with the historical EMT signal modified with an extreme warming climatological change. Consequently, the absence of MHW during this period could be attributed to the exceptional EMT conditions which have likely lowered the sea surface temperatures and increased the vertical mixing in the Adriatic Sea and, hence, prevented extreme warming episodes under historical and RCP8.5 conditions. Further, as the EMT is known to alter the thermohaline circulation, it may have strengthened cold-water upwelling or changed stratification patterns, leading to reduced heat retention at the surface. This disruption would have also limited the formation and persistence of MHWs in the Adriatic Sea during that period.

The presence of a gap in MHW activity visible under both historical and RCP8.5 conditions thus suggests that natural variability, such as the EMT, plays a significant role in modulating heatwave occurrences in the Adriatic, even under strong anthropogenic forcing. However, the study of Soto-Navarro et al. (2020) found that most Med-CORDEX regional climate models project a reduction of the dense water formation in the Aegean Sea and, hence, of EMT-like situations. Finally, the suppression of MHW in the Adriatic Sea has not been previously linked to the EMT.

As EMT events lead to episodic and significant shifts in water properties, whereas BiOS represents a more gradual oscillatory pattern, these results suggest that while some large-scale circulation changes (like EMT) might influence MHW occurrence, others (like BiOS) may not exert a strong enough effect to suppress or enhance MHWs directly. Consequently, further targeted research is necessary to establish a definitive connection between MHW intensities and frequencies and EMT or other significant oceanographic events like the BiOS.

5 Conclusions

This study provides a comprehensive analysis of marine heatwaves (MHWs) in the Adriatic Sea under both historical (1987–2017) and far-future extreme warming (2070–2100, RCP8.5) scenarios utilizing the high-resolution Adriatic Sea and Coast (AdriSC) climate model. By employing the pseudo-global-warming (PGW) approach, the research offers valuable insights into the projected changes in MHW characteristics, their environmental drivers, and the implications for marine ecosystems and coastal communities. The findings highlight the increasing intensity and spatial extent of MHWs under extreme warming, while also revealing the limitations and strengths of the PGW methodology in simulating these events. The five key findings of the study are as follows.

First, under the RCP8.5 scenario, MHWs in the Adriatic Sea are projected to become significantly more intense, with mean cumulative intensities increasing by approximately 6 times compared to historical conditions. The spatial extent of these events also expands, particularly in the central and eastern Adriatic regions. The cumulative heat index (CHI) reveals that far-future MHWs will consistently exceed historical extremes, with values peaking at nearly 48×10^5 °C km^2 d compared to 9×10^5 °C km^2 d in the historical period. This indicates a substantial rise in the severity of MHWs, posing greater risks to marine ecosystems and human activities.

Second, MHWs under both historical and far-future conditions exhibit strong seasonal patterns, with the most intense events occurring between May and September. However, under RCP8.5, extreme MHWs are also projected to extend into late autumn and early winter, particularly in the northern Adriatic and along the Italian coast. The spatial distribution of MHWs remains consistent, with the deepest parts of the Adriatic experiencing the highest number of events. However, the nearshore areas, which are critical for aquaculture and tourism, are also significantly affected, albeit with fewer events.

Third, air–sea heat fluxes play an important role in the onset of MHWs. This influence is particularly strong in the northern Adriatic and along the Italian coast, where freshwater discharge from the Po River affects stratification, water quality, and heat distribution. Under extreme warming, the influence of air–sea fluxes during the decline phase of MHWs increases, indicating a shift in the dynamics of heat dissipation. However, future MHWs are expected to have the same duration as under the historical conditions despite this altered heat exchange processes.

Fourth, the Po River plume significantly influences MHW dynamics, particularly in the northern Adriatic and along the Italian coast. However, the results presented in this study are not aligned with the previously published literature as the AdriSC simulations account for the changes in optical properties along the Po River plume, which carries a lot of suspended sediments and organic matter. Consequently, it is found that lower river discharge is associated with the onset of intense MHWs, as reduced stratification and increased solar penetration enhance surface warming. Conversely, higher discharge during the decline phase helps dissipate heat, mitigating the persistence of MHWs. Under RCP8.5, the anti-correlation between Po River discharge and MHW intensity strengthens, highlighting the river's role in modulating heatwave dynamics under extreme warming.

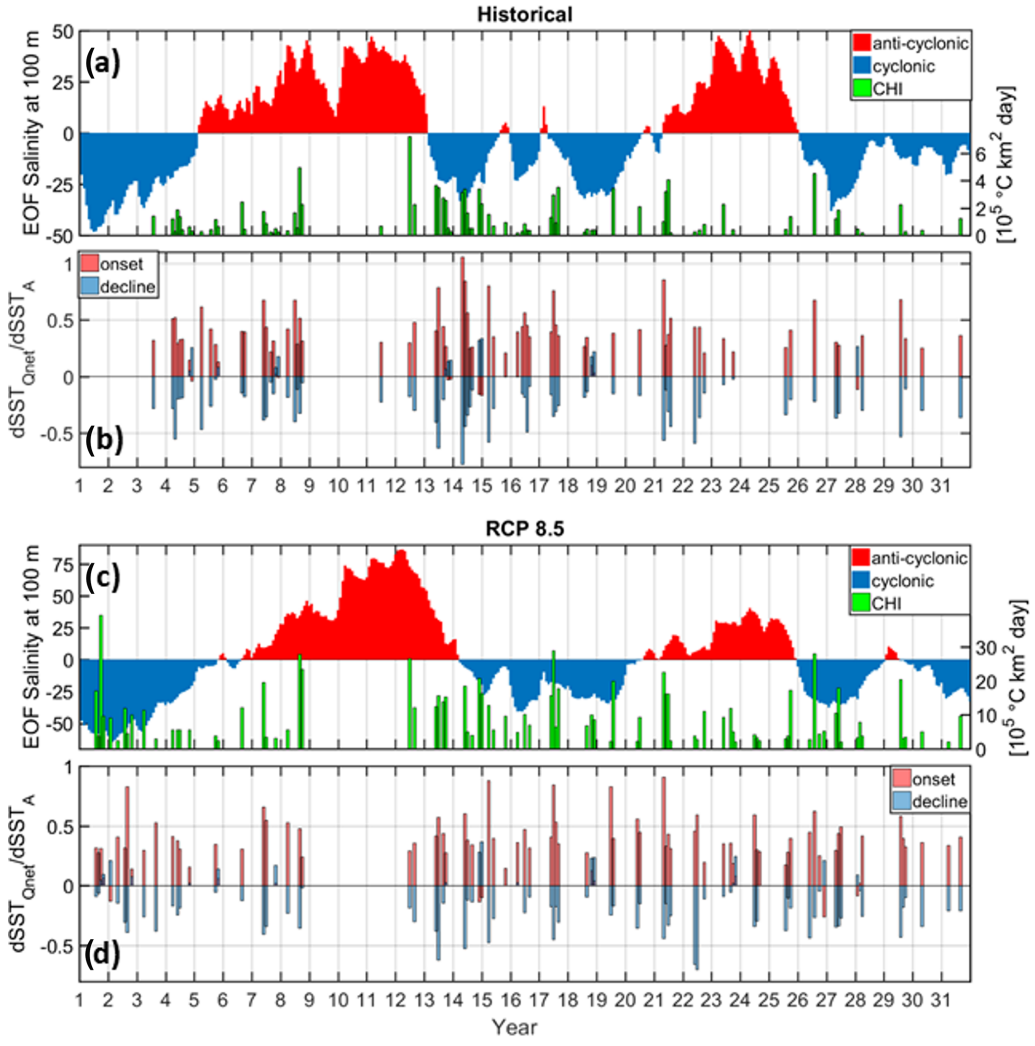

Figure 13. Monthly time series over the 31-year historical **(a, b)** and RCP8.5 **(c, d)** periods, as well as CHI – extracted from the detrended Adriatic SST – superimposed on the first empirical orthogonal function (EOF) of salinity at 100 m depth representing the influence of the BiOS in the Adriatic Sea **(a, c)**. Contribution of total air–sea heat fluxes ($dSST_{Q_{net}}$) to the change in sea surface temperature anomaly ($dSST_A$) during MHW onset and decline phases.

Finally, for both simulations, the study identifies, for the very first time, a gap in MHW activity during the Eastern Mediterranean Transient (EMT). This event seems to suppress MHWs by enhancing vertical mixing and lowering sea surface temperatures. However, while these results seem to demonstrate the influence of natural variability on MHWs, no correlation was found with the Ionian–Adriatic Bimodal Oscillating System (BiOS), highlighting the need for further research to clarify the role of oceanographic events in Adriatic MHW dynamics.

Based on these results, the added value of the PGW approach – which effectively captures the thermodynamic changes associated with extreme warming – has been clearly demonstrated. However, PGW assumes stationarity in climate signals, potentially oversimplifying the evolving dynamics of MHWs. Furthermore, the one-way coupling between the atmosphere and ocean in the AdriSC model restricts the representation of feedback mechanisms which could influence MHW intensity and frequency. Future improvements in model coupling are thus necessary to enhance the accuracy of Adriatic MHW projections.

In conclusion, this study advances our understanding of MHWs in the Adriatic Sea under one extreme warming scenario, highlighting the critical role of high-resolution modelling in predicting future climate impacts. While the PGW approach provides valuable insights, its limitations emphasize the need for continued refinement of climate models and methodologies. Additionally, to provide a more comprehensive understanding of the cumulative impacts on marine ecosystems and to better represent the climate uncertainties, MHW projections under various scenarios should be derived by using an ensemble of PGW forcing and combined with

assessments of other climate stressors, such as ocean acidification and deoxygenation.

Overall, the projected increase in MHW intensity and spatial extent under the ongoing and future climate warming will pose significant threats to Adriatic marine ecosystems, including habitat degradation, biodiversity loss, and shifts in species distribution. Coastal communities reliant on fisheries and aquaculture will face heightened risks, as MHWs can lead to mass mortality events and disrupt marine resource availability. The findings thus underscore the urgent need to engage local stakeholders, including fisheries, aquaculture operators, and coastal managers in the development of adaptive strategies to mitigate these impacts, particularly in vulnerable nearshore areas.

Code availability. The code of the COAWST model as well as the ecFlow pre-processing scripts and the input data needed to re-run the AdriSC climate model can be obtained from the Open Science Framework (OSF) data repository (https://doi.org/10.17605/OSF.IO/ZB3CM, Denamiel, 2021) under the MIT license.

Data availability. The model results used to produce this article can be obtained from the Open Science Framework (OSF) FAIR data repository (https://doi.org/10.17605/OSF.IO/FHWXJ, Denamiel, 2025a) under the CC-By Attribution 4.0 International license.

Video supplement. Movies S1 and S2 are available at https://doi.org/10.17605/OSF.IO/EJ8GQ (Denamiel, 2025b; under the CC-By Attribution 4.0 International license). Movie S1 shows an animation of the historical (1987–2017) Adriatic marine heatwave mean intensity, duration, and category extracted from the AdriSC model. Movie S2 shows an animation of the RCP8.5 (2070–2100) Adriatic marine heatwave mean intensity, duration, and category extracted from the AdriSC model.

Competing interests. The author has declared that there are no competing interests.

Disclaimer. Publisher's note: Copernicus Publications remains neutral with regard to jurisdictional claims made in the text, published maps, institutional affiliations, or any other geographical representation in this paper. While Copernicus Publications makes every effort to include appropriate place names, the final responsibility lies with the authors.

Acknowledgements. The author would like to sincerely thank the anonymous reviewer and Justino Martinez for their thorough and constructive reviews. Their insightful comments and suggestions greatly helped improve the clarity, structure, and scientific quality of this paper. The computing and archive facilities used in this research were provided by the European Centre for Medium-Range Weather Forecasts (ECMWF) through the Croatian national quota and the ECMWF Special Projects "The Adriatic decadal and inter-annual oscillations: modelling component" and "Numerical modelling of the Adriatic–Ionian decadal and inter-annual oscillations: from realistic simulations to process-oriented experiments".

Financial support. The research has been supported by the HORIZON EUROHPC JU project ChEESE-2P (grant no. 101093038).

Review statement. This paper was edited by Aida Alvera-Azcárate and reviewed by Justino Martínez and one anonymous referee.

References

Akpinar, A., Yilmaz, E., Fach, B., and Salihoglu, B.: Physical oceanography of the Eastern Mediterranean Sea, in: The Turkish Part of the Mediterranean Sea, edited by: Turan, K., Salihoglu, B., Ozbek, E. O., and Ozturk, B., Turkish Marine Research Foundation, Turkey, 1–14, 2016.

Amaya, D. J., Jacox, M. G., Fewings, M. R., Saba, V. S., Stuecker, M. F., Rykaczewski, R. R., Ross, A. C., Stock, C. A., Capotondi, A., Petrik, C. M., Bograd, S. J., Alexander, M. A., Cheng, W., Hermann, A. J., Kearney, K. A., and Powell, B. S.: Marine heatwaves need clear definitions so coastal communities can adapt, Nature, 616, 29–32, https://doi.org/10.1038/d41586-023-00924-2, 2023.

Beuvier, J., Sevault, F., Herrmann, M., Kontoyiannis, H., Ludwig, W., Rixen, M., Stanev, E., Béranger, K., and Somot, S.: Modeling the Mediterranean Sea interannual variability during 1961–2000: Focus on the Eastern Mediterranean Transient, J. Geophys. Res.-Atmos., 115, C08017, https://doi.org/10.1029/2009JC005950, 2010.

Bonaldo, D., Carniel, S., Colucci, R. R., Denamiel, C., Pranić, P., Raicich, F., Ricchi, A., Sangelantoni, L., Vilibić, I., and Vitelletti, M. L.: AdriE: a high-resolution ocean model ensemble for the Adriatic Sea under severe climate change conditions, Ocean Sci., 21, 1003–1031, https://doi.org/10.5194/os-21-1003-2025, 2025.

Bowman, A. and Azzalini, A.: Applied Smoothing Techniques for Data Analysis: The Kernel Approach with S-Plus Illustrations, Oxford Univ. Press, ISBN 978-0198523963, 1997.

Bracchetti, L., Capriotti, M., Fazzini, M., Cocci, P., and Palermo, F. A.: Mass Mortality Event of Mediterranean Mussels (Mytilus galloprovincialis) in the Middle Adriatic: Potential Implications of the Climate Crisis for Marine Ecosystems, Diversity, 16, 130, https://doi.org/10.3390/d16030130, 2024.

Brogli, R., Heim, C., Mensch, J., Sørland, S. L., and Schär, C.: The pseudo-global-warming (PGW) approach: methodology, software package PGW4ERA5 v1.1, validation, and sensitivity analyses, Geosci. Model Dev., 16, 907–926, https://doi.org/10.5194/gmd-16-907-2023, 2023.

Bujosa Mateu, A., Alegre Latorre, L., Comas, M. V., Salom, J., García Gasalla, M., Planas Bibiloni, L., Orfila Timoner, J., and Murillas Angoiti, J.: Impact of heat waves on human morbidity and hospital admissions in a city of the western

mediterranean area, Int. Arch. Occ. Env. Hea., 97, 757–765 https://doi.org/10.1007/s00420-024-02082-y, 2024.

Copernicus Climate Change Service (C3S): European State of the Climate 2023, https://climate.copernicus.eu/esotc/2023 (last access: 13 March 2025), 2023.

Dayan, H., McAdam, R., Speich, S., and Masina, S.: Diversity of marine heatwave trends across the Mediterranean Sea over the last decades, in: Copernicus ocean state report, issue 6, J. Oper. Oceanogr., 15, 1–220, https://doi.org/10.1080/1755876X.2022.2095169, 2022.

Dayan, H., McAdam, R., Juza, M., Masina, S., and Speich, S.: Marine heat waves in the Mediterranean Sea: An assessment from the surface to the subsurface to meet national needs, Front. Mar. Sci., 10, 1045138, https://doi.org/10.3389/fmars.2023.1045138, 2023.

Dee, D. P., Uppala, S. M., Simmons, A. J., Berrisford, P., Poli, P., Kobayashi, S., Andrae, U., Balmaseda, M. A., Balsamo, G., Bauer, P., Bechtold, P., Beljaars, A. C. M., van de Berg, L., Bidlot, J., Bormann, N., Delsol, C., Dragani, R., Fuentes, M., Geer, A. J., Haimberger, L., Healy, S. B., Hersbach, H., Hólm, E. V., Isaksen, L., Kållberg, P., Köhler, M., Matricardi, M., McNally, A. P., Monge-Sanz, B. M., Morcrette, J.-J., Park, B.-K., Peubey, C., de Rosnay, P., Tavolato, C., Thépaut, J.-N., and Vitart, F.: The ERA-Interim reanalysis: configuration and performance of the data assimilation system, Q. J. Roy. Meteor. Soc., 137, 553–597, https://doi.org/10.1002/qj.828, 2011.

Denamiel, C.: AdriSC Climate Model: Evaluation Run, OSF [code], https://doi.org/10.17605/OSF.IO/ZB3CM, 2021.

Denamiel, C.: Adriatic Marine Heatwaves extracted from the AdriSC climate model under historical and RCP 8.5 conditions, OSF [data set], https://doi.org/10.17605/OSF.IO/FHWXJ, 2025a.

Denamiel, C.: Animation of the Adriatic Marine Heatwaves extracted from the AdriSC climate model under historical and RCP 8.5 conditions, OSF [video], https://doi.org/10.17605/OSF.IO/EJ8GQ, 2025b.

Denamiel, C., Šepić, J., Ivanković, D., and Vilibić, I.: The Adriatic Sea and Coast modelling suite: Evaluation of the meteotsunami forecast component, Ocean Model., 135, 71–93, https://doi.org/10.1016/j.ocemod.2019.02.003, 2019.

Denamiel, C., Pranić, P., Quentin, F., Mihanović, H., and Vilibić, I.: Pseudo-global warming projections of extreme wave storms in complex coastal regions: The case of the Adriatic Sea, Clim. Dynam., 55, 2483–2509, https://doi.org/10.1007/s00382-020-05397-x, 2020a.

Denamiel, C., Tojčić, I., and Vilibić, I.: Far future climate (2060–2100) of the northern Adriatic air–sea heat transfers associated with extreme bora events, Clim. Dynam., 55, 3043–3066, https://doi.org/10.1007/s00382-020-05435-8, 2020b.

Denamiel, C., Pranić, P., Ivanković, D., Tojčić, I., and Vilibić, I.: Performance of the Adriatic Sea and Coast (AdriSC) climate component – a COAWST V3.3-based coupled atmosphere–ocean modelling suite: atmospheric dataset, Geosci. Model Dev., 14, 3995–4017, https://doi.org/10.5194/gmd-14-3995-2021, 2021a.

Denamiel, C., Tojčić, I., and Vilibić, I.: Balancing accuracy and efficiency of atmospheric models in the northern Adriatic during severe bora events, J. Geophys. Res.-Oceans, 126, e2020JD033516, https://doi.org/10.1029/2020JD033516, 2021b.

Denamiel, C., Tojčić, I., Pranić, P., and Vilibić, I.: Modes of the BiOS-driven Adriatic Sea thermohaline variability, Clim. Dynam., 59, 1097–1113, https://doi.org/10.1007/s00382-022-06178-4, 2022.

Denamiel, C., Tojčić, I., and Pranić, P.: A new vision of the Adriatic Dense Water future under extreme warming, Ocean Sci., 21, 37–62, https://doi.org/10.5194/os-21-37-2025, 2025.

Denaxa, D., Korres, G., Bonino, G., Masina, S., and Hatzaki, M.: The role of air–sea heat flux for marine heatwaves in the Mediterranean Sea, in: 8th edition of the Copernicus Ocean State Report (OSR8), edited by: von Schuckmann, K., Moreira, L., Grégoire, M., Marcos, M., Staneva, J., Brasseur, P., Garric, G., Lionello, P., Karstensen, J., and Neukermans, G., Copernicus Publications, State Planet, 4-osr8, 11, https://doi.org/10.5194/sp-4-osr8-11-2024, 2024.

Deser, C., Phillips, A. S., Alexander, M. A., Amaya, D. J., Capotondi, A., Jacox, M. G., and Scott, J. D.: Future Changes in the Intensity and Duration of Marine Heat and Cold Waves: Insights from Coupled Model Initial-Condition Large Ensembles, J. Climate, 37, 1877–1902, https://doi.org/10.1175/JCLI-D-23-0278.1, 2024.

Fischer, E. and Schär, C.: Consistent geographical patterns of changes in high-impact European heatwaves, Nat. Geosci., 3, 398–403, https://doi.org/10.1038/ngeo866, 2010.

Garrabou, J., Coma, R., Bensoussan, N., Bally, M., Chevaldonné, P., Cigliano M., Diaz, D., Harmelin, J. G., Gambi, M. C., Kersting, D. K., Ledoux, J. B., Lejeusne, C., Linares, C., Marschal, C., Pérez, T., Ribes, M., Romano, J. C., Serrano, E., Teixido, N., Torrents, O., Zabala, M., Zuberer, F., and Cerrano, C.: Mass mortality in northwestern mediterranean rocky benthic communities: effects of the 2003 heat wave, Glob. Change Biol., 15, 1090–1103, https://doi.org/10.1111/j.1365-2486.2008.01823.x, 2009.

Garrabou, J., Gómez-Gras, D., Ledoux, J.-B., Linares, C., Bensoussan, N., López-Sendino, P., Bazairi, H., Espinosa, F., Ramdani, M., Grimes, S., Benabdi, M., Souissi, J. B., Soufi, E., Khamassi, F., Ghanem, R., Ocaña, O., Ramos-Esplà, A., Izquierdo, A., Anton, I., Rubio-Portillo, E., Barbera, C., Cebrian, E., Marbà, N., Hendriks, I. E., Duarte, C. M., Deudero, S., Díaz, D., Vázquez-Luis, M., Alvarez, E., Hereu, B., Kersting, D. K., Gori, A., Viladrich, N., Sartoretto, S., Pairaud, I., Ruitton, S., Pergent, G., Pergent-Martini, C., Rouanet, E., Teixidó, N., Gattuso, J.-P., Fraschetti, S., Rivetti, I., Azzurro, E., Cerrano, C., Ponti, M., Turicchia, E., Bavestrello, G., Cattaneo-Vietti, R., Bo, M., Bertolino, M., Montefalcone, M., Chimienti, G., Grech, D., Rilov, G., Tuney Kizilkaya, I., Kizilkaya, Z., Eda Topçu, N., Gerovasileiou, V., Sini, M., Bakran-Petricioli, T., Kipson, S., and Harmelin, J. G.: Collaborative Database to Track Mass Mortality Events in the Mediterranean Sea, Front. Mar. Sci., 6, 707, https://doi.org/10.3389/fmars.2019.00707, 2019.

Garrabou, J., Gómez-Gras, D., Medrano, A., Cerrano, C., Ponti, M., Schlegel, R., Bensoussan, N., Turicchia, E., Sini, M., Gerovasileiou, V., Teixido, N., Mirasole, A., Tamburello, L., Cebrian, E., Rilov, G., Ledoux, J.-B., Souissi, J. B., Khamassi, F., Ghanem, R., and Harmelin, J.-G.: Marine heatwaves drive recurrent mass mortalities in the Mediterranean Sea, Glob. Change Biol., 28, 5708–5725, https://doi.org/10.1111/gcb.16301, 2022.

Gilbert, R. O.: Statistical methods for environmental pollution monitoring, Wiley, New York, ISBN 0-442-23050-8, 1987.

Hansen, J., Sato, M., Kharecha, P., and von Schuckmann, K.: Earth's energy imbalance and implications, Atmos. Chem. Phys., 11, 13421–13449, https://doi.org/10.5194/acp-11-13421-2011, 2011.

Heim, C., Schlemmer, L., and Schär, C.: Application of the pseudo-global warming approach in a kilometer-resolution climate simulation of the tropics, J. Geophys. Res.-Atmos., 128, e2022JD037958, https://doi.org/10.1029/2022JD037958, 2023.

Hobday, A. J., Alexander, L. V., Perkins, S. E., Smale, D. A., Straub, S. C., Oliver, E. C. J., Benthuysen, J. A., Burrows, M. T., Donat, M. G., Feng, M., Holbrook, N. J., Moore, P. J., Scannell, H. A., Sen Gupta, A., Wernberg, T.: A hierarchical approach to defining marine heatwaves, Prog. Oceanogr., 141, 227–238, https://doi.org/10.1016/j.pocean.2015.12.014, 2016.

Hobday, A. J., Oliver, E. C. J., Sen Gupta, A., Benthuysen, J. A., Burrows, M. T., Donat, M. G., Holbrook, N. J., Moore, P. J., Thomsen, M. S., Wernberg, T., and Smale, D. A.: Categorizing and naming marine heatwaves, Oceanography, 31, 162–173, https://doi.org/10.5670/oceanog.2018.205, 2018.

Hourdin, F., Musat, I., Bony, S., Braconnot, P., Codron, F., Dufresne, J. L., Fairhead, L., Filiberti, M. A., Friedlingstein, P., Grandpeix, J. Y., Krinner, G., LeVan, P., Li, Z. X., and Lott, F.: The LMDZ4 general circulation model: climate performance and sensitivity to parametrized physics with emphasis on tropical convection, Clim. Dynam., 27, 787–813, https://doi.org/10.1007/s00382-006-0158-0, 2006.

Imada, Y., Watanabe, M., Kawase, H., Shiogama, H., and Arai, M.: The July 2018 High Temperature Event in Japan Could Not Have Happened without Human-Induced Global Warming, SOLA, 15A, 8–12, https://doi.org/10.2151/sola.15A-002, 2019.

Juza, M., Fernández-Mora, À., and Tintoré, J.: Sub-Regional marine heat waves in the Mediterranean Sea from observations: Long-term surface changes, Sub-surface and coastal responses, Front. Mar. Sci., 9, 785771, https://doi.org/10.3389/fmars.2022.785771, 2022.

Kendall, M. G.: Rank correlation methods, 4th Edn., Charles Griffin, London, https://archive.org/details/rankcorrelationm0000kend, 1975.

Klein, B., Roether, W., Manca, B. B., Bregant, D., Beitzel, V., Kovacevic, V., and Luchetta, A.: The large deep water transient in the Eastern Mediterranean, Deep-Sea Res. Pt. I, 46, 371–414, https://doi.org/10.1016/s0967-0637(98)00075-2, 1999.

Konsta, K., Doxa, A., Katsanevakis, S., and Mazaris, A. D.: Projected marine heatwaves over the Mediterranean Sea and the network of marine protected areas: a three-dimensional assessment, Climatic Change, 178, 17, https://doi.org/10.1007/s10584-025-03860-4, 2025.

Laprise, R.: The Euler Equations of motion with hydrostatic pressure as independent variable, Mont. Weather Rev., 120, 197–207, https://doi.org/10.1175/1520-0493(1992)120<0197:TEEOMW>2.0.CO;2, 1992.

Li, P. and Tanhua, T.: Recent changes in deep ventilation of the Mediterranean Sea; Evidence from long-term transient tracer observations, Front. Mar. Sci., 7, 594, https://doi.org/10.3389/fmars.2020.00594, 2020.

Mann, H. B.: Non-parametric tests against trend, Econometrica1, 3, 163–171, 1945.

Martín, M. L., Calvo-Sancho, C., Taszarek, M., González-Alemán, J. J., Montoro-Mendoza, A., Díaz-Fernández, J., Bolgiani, P., Sastre, M., and Martín, Y.: Major role of marine heatwave and anthropogenic climate change on a Giant hail Event in Spain, Geophys. Res. Lett., 51, e2023GL107632, https://doi.org/10.1029/2023GL107632, 2024.

Martínez, J., Leonelli, F. E., García-Ladona, E., Garrabou, J., Kersting, D. K., Bensoussan, N., and Pisano, A.: Evolution of marine heatwaves in warming seas: the Mediterranean Sea case study, Front. Mar. Sci., 10, 1193164, https://doi.org/10.3389/fmars.2023.1193164, 2023.

Masselot, P., Mistry, M. N., Rao, S., Huber, V., Monteiro, A., Samoli, E., Stafoggia, M., de'Donato, F., Garcia-Leon, D., Ciscar, J.-C., Feyen, L., Schneider, A., Katsouyanni, K., Vicedo-Cabrera, A. M., Aunan, K., and Gasparrini, A.: Estimating future heat-related and cold-related mortality under climate change, demographic and adaptation scenarios in 854 European cities, Nat. Med., 31, 1294–1302, https://doi.org/10.1038/s41591-024-03452-2, 2025.

Merryfield, W. J.: Origin of Thermohaline Staircases, J. Phys. Oceanogr., 30, 1046–1068, https://doi.org/10.1175/1520-0485(2000)030<1046:OOTS>2.0.CO;2, 2000.

Mondal, A., Kundu, S., and Mukhopadhyay, A.: Rainfall trend analysis by Mann-Kendall test: a case study of north-eastern part of Cuttack district, Orissa, Int. J. Geol. Earth Environ Sci., 2, 70–78, 2012.

Olita, A., Sorgente, R., Natale, S., Gaberšek, S., Ribotti, A., Bonanno, A., and Patti, B.: Effects of the 2003 European heatwave on the Central Mediterranean Sea: surface fluxes and the dynamical response, Ocean Sci., 3, 273–289, https://doi.org/10.5194/os-3-273-2007, 2007.

Pastor, F., Paredes-Fortuny, L., and Khodayar, S.: Mediterranean marine heatwaves intensify in the presence of concurrent atmospheric heatwaves, Commun. Earth Environ., 5, 797, https://doi.org/10.1038/s43247-024-01982-8, 2024.

Patricola, C. M., and Wehner, M.F.: Anthropogenic influences on major tropical cyclone events, Nature, 563, 339–346, https://doi.org/10.1038/s41586-018-0673-2, 2018.

Perkins-Kirkpatrick, S. E. and Lewis, S. C.: Increasing trends in regional heatwaves, Nat. Commun., 11, 3357, https://doi.org/10.1038/s41467-020-16970-7, 2020.

Pranić, P., Denamiel, C., and Vilibić, I.: Performance of the Adriatic Sea and Coast (AdriSC) climate component – a COAWST V3.3-based one-way coupled atmosphere–ocean modelling suite: ocean results, Geosci. Model Dev., 14, 5927–5955, https://doi.org/10.5194/gmd-14-5927-2021, 2021.

Pranić, P., Denamiel, C., Janeković, I., and Vilibić, I.: Multi-model analysis of the Adriatic dense-water dynamics, Ocean Sci., 19, 649–670, https://doi.org/10.5194/os-19-649-2023, 2023.

Pranić, P., Denamiel, C., and Vilibić, I.: Kilometer-scale assessment of the Adriatic dense water multi-decadal dynamics, J. Geophys. Res.-Oceans, 129, e2024JC021182, https://doi.org/10.1029/2024JC021182, 2024.

Radko, T., Bulters, A., and Flanagan, J. D.: Double-diffusive recipes. Part I: Large-scale dynamics of thermohaline staircases, J. Phys. Oceanogr., 44, 1269–1284, https://doi.org/10.1175/JPO-D-13-0155.1, 2014.

Roether, W., Manca, B. B., Klein, B., Bregant, D., Georgopoulos, D., Beitzel, V., Beitzel, V., Kovačević, V., and Luchetta, A.: Recent changes in eastern Mediterranean deep waters, Science, 271, 333–335, https://doi.org/10.1126/science.271.5247.333, 1996.

Roether, W., Klein, B., Manca, B. B., Theocharis, A., and Kioroglou, S.: Transient Eastern Mediterranean deep waters in response to themassive dense-water output of the Aegean Sea in the 1990's, Prog. Oceanogr., 74, 540–571, https://doi.org/10.1016/j.pocean.2007.03.001, 2007.

Salini, R., Tora, S., Filipponi, F., Conte, A., Giansante, C., and Ippoliti, C.: Analyzing trend and heatwaves of 15 Years of Sea-surface Temperature Variations along the Italian Adriatic Coast, Vet. Ital., 60, https://doi.org/10.12834/VetIt.3583.27524.2, 2024.

Sani, T., Marini, M., Campanelli, A., Machado Toffolo, M., Goffredo, S., and Grilli, F.: Evolution of Freshwater Runoff in the Western Adriatic Sea over the Last Century, Environments, 11, 22, https://doi.org/10.3390/environments11010022, 2024.

Schär, C., Frei, C., Luthi, D., and Davies, H. C.: Surrogate climate-change scenarios for regional climate models, Geophys. Res. Lett., 23, 669–672, https://doi.org/10.1029/96GL00265, 1996.

Schlegel, R. W., Oliver, E. C. J., Wernberg, T. W., and Smit, A. J.: Nearshore and offshore co-occurrences of marine heatwaves and cold-spells, Prog. Oceanogr., 151, 189–205, 2017.

Schlegel, R. W., Oliver, E. C. J., and Chen, K.: Drivers of Marine Heatwaves in the Northwest Atlantic: The Role of Air–Sea Interaction During Onset and Decline, Front. Mar. Sci., 8, 1–18, https://doi.org/10.3389/fmars.2021.627970, 2021.

Shchepetkin, A. F. and McWilliams, J. C.: Correction and commentary for "Ocean forecasting in terrain-following coordinates: Formulation and skill assessment of the regional ocean modeling system" by Haidvogel et al., Journal of Computational Physics, 227, pp. 3595–3624, J. Comput. Phys., 228, 8985–9000, https://doi.org/10.1016/j.jcp.2009.09.002, 2009.

Simoncelli, S., Fratianni, C., Pinardi, N., Grandi, A., Drudi, M., Oddo, P., and Dobricic, S.: Mediterranean Sea Physical Reanalysis (CMEMS MED-Physics), Version 1, Copernicus Monitoring Environment Marine Service (CMEMS) [data set], https://doi.org/10.25423/MEDSEA_REANALYSIS_PHYS_006_004, 2019.

Skamarock, W. C., Klemp, J. B., Dudhia, J., Gill, D. O., Barker, D. M., Wang, W., and Powers, J. G.: A description of the Advanced Research WRF Version 2, NCAR Technical Note NCAR/TN468+STR, https://doi.org/10.5065/D6DZ069T, 2005.

Smale, D. A., Wernberg, T., Oliver, E. C. J., Thomsen, M., Harvey, B. P., Straub, S. C., Burrows, M. T., Alexander, L. V., Benthuysen, J. A., Donat, M. G., Feng, M., Hobday, A. J., Holbrook, N. J., Perkins-Kirkpatrick, S. E., Scannell, H. A., Sen Gupta, A., Payne, B. L., and Moore, P. J.: Marine heatwaves threaten global biodiversity and the provision of ecosystem services, Nat. Clim. Change, 9, 306–312, https://doi.org/10.1038/s41558-019-0412-1, 2019.

Smith, K. E., Aubin, M., Burrows, M. T., Filbee-Dexter, K., Hobday, A. J., Holbrook, N. J., King, N. G., Moore, P. J., Sen Gupta, A., Thomsen, M., Wernberg, T., Wilson, E., and Smale, D. A.: Global impacts of marine heatwaves on coastal foundation species, Nat. Commun., 15, 5052, https://doi.org/10.1038/s41467-024-49307-9, 2024.

Smith, K. E., Sen Gupta, A., Amaya, D., Benthuysen, J. A., Burrows, M. T., Capotondi, A., Filbee-Dexter, K., Frölicher, T. L., Hobday, A. J., Holbrook, N. J., Malan, N., Moore, P. J., Oliver, E. C. J., Richaud, B., Salcedo-Castro, J., Smale, D. A., Thomsen, M., and Wernberg, T.: Baseline matters: Challenges and implications of different marine heatwave baselines, Prog. Oceanogr., 231, 103404, https://doi.org/10.1016/j.pocean.2024.103404, 2025.

Soto-Navarro, J., Jordá, G., Amores, A., Cabos, W., Somot, S., Sevault, F., Macias, D., Djurdjevic, V., Sannino, G., Li, L., and Sein, D.: Evolution of Mediterranean Sea water properties under climate change scenarios in the Med-CORDEX ensemble, Clim. Dynam., 54, 2135–2165, https://doi.org/10.1007/s00382-019-05105-4, 2020.

Sparnocchia, S., Schiano, M. E., Picco, P., Bozzano, R., and Cappelletti, A.: The anomalous warming of summer 2003 in the surface layer of the Central Ligurian Sea (Western Mediterranean), Ann. Geophys., 24, 443–452, https://doi.org/10.5194/angeo-24-443-2006, 2006.

Tejedor, E., Benito, G., Serrano-Notivoli, R., González-Rouco, F., Esper, J. and Büntgen, U.: Recent heatwaves as a prelude to climate extremes in the western Mediterranean region, Clim. Atmos. Sci., 7, 218, https://doi.org/10.1038/s41612-024-00771-6, 2024.

Tojčić, I., Denamiel, C., and Vilibić, I.: Kilometer-scale trends and variability of the Adriatic present climate (1987–2017), Clim. Dynam., 61, 2521–2545, https://doi.org/10.1007/s00382-023-06700-2, 2023.

Tojčić, I., Denamiel, C., and Vilibić, I.: Kilometer-scale trends, variability, and extremes of the Adriatic far-future climate (RCP 8.5, 2070–2100), Front. Mar. Sci., 11, 1329020, https://doi.org/10.3389/fmars.2024.1329020, 2024.

Trenberth, K. E., Cheng, L., Jacobs, P., Zhang, Y., and Fasullo, J.: Hurricane Harvey links to ocean heat content and climate change adaptation, Earth's Future, 6, 730–744, https://doi.org/10.1029/2018EF000825, 2018.

Velaoras, D., Papadopoulos, V. P., Kontoyiannis, H., Papageorgiou, D. K., and Pavlidou, A.: The response of the Aegean Sea (eastern Mediterranean) to the extreme 2016–2017 winter, Geophys. Res. Lett., 44, 9416–9423, https://doi.org/10.1002/2017gl074761, 2017.

Verri, G., Furnari, L., Gunduz, M., Senatore, A., Santos da Costa, V., De Lorenzis, A., Fedele, G., Manco, I., Mentaschi, L., Clementi, E., Coppini, G., Mercogliano, P., Mendicino, G., and Pinardi, N.: Climate projections of the Adriatic Sea: role of river release, Front. Clim., 6, 1368413, https://doi.org/10.3389/fclim.2024.1368413, 2024.

von Schuckmann, K., Palmer, M., Trenberth, K., Cazenave, A., Chambers, D., Champollion, N., Hansen, J., Josey, S. A., Loeb, N., Mathieu, P.-P., Meyssignac, B. and Wild, M.: An imperative to monitor Earth's energy imbalance, Nat. Clim. Change, 6, 138–144, https://doi.org/10.1038/nclimate2876, 2016.

Warner, J. C., Armstrong, B., He, R., and Zambon, J. B.: Development of a Coupled Ocean-Atmosphere-Wave-Sediment Transport (COAWST) modeling system, Ocean Modell., 35, 230–244, https://doi.org/10.1016/j.ocemod.2010.07.010, 2010.

Xue, Z., Ullrich, P., and Leung, L.-Y. R.: Sensitivity of the pseudo-global warming method under flood conditions: a case study from the northeastern US, Hydrol. Earth Syst. Sci., 27, 1909–1927, https://doi.org/10.5194/hess-27-1909-2023, 2023.

Zemunik Selak, P., Denamiel, C., Peharda, M., Schöne, B. R., Thébault, J., Uvanović, H., Markulin, K., and Vilibić, I.: Projecting expected growth period of bivalves in a coastal temperate sea, Limnol. Oceanogr. Lett., 9, 815–826, https://doi.org/10.1002/lol2.10393, 2024.